PHOTOEMISSION STUDIES OF METALLIC NICKEL

Mr. JiangYang

A Thesis Submitted in Partial Fulfillment of the Requirements

for the Degree of Master of Science in Physics

Suranaree University of Technology

Academic Year 1999

ISBN 974-7359-49-9

การศึกษาโลหะนิเกิลโดยวิธีการโฟโตอิมิชชัน

Mr. Jiang Yang

วิทยานิพนธ์นี้เป็นส่วนหนึ่งของการศึกษาตามหลักสูตรปริญญาวิทยาศาสตรมหาบัณฑิต

สาขาวิชาฟิสิกส์

มหาวิทยาลัยเทคโนโลยีสุรนารี

ปีการศึกษา 2542

ISBN 974-7359-49-9

Thesis Title

Photoemission Studies of Metallic Nickel

Suranaree University of Technology Council has approved this thesis submitted in partial fulfillment of the requirements for a Master's Degree.

Thesis Examining Committee

……
(Assoc. Prof. Dr. Weerapong Pairsuwan)
Chairman

……
(Prof. Dr. Takehiko Ishii)
Thesis Advisor

……
(Dr. Prayoon Songsiriritthigul)
Member

……. ……
(Assoc. Prof. Dr. Kasem Prabriputaloong) (Assoc. Prof. Dr. Tassanee Sukosol)
Vice Rector for Academic Affairs Dean / Institute of Science

Mr. Jiang Yang: การศึกษาโลหะนิเกิลโดยวิธีการโฟโตอิมิชชัน (PHOTOEMISSION STUDIES OF METALLIC NICKEL) อาจารย์ที่ปรึกษา: PROF. TAKEHIKO ISHII, Ph.D. 81 หน้า
ISBN 974-7359-49-9

การทดลองทางด้านโฟโตอิมิชชันได้นำไปใช้ในการยืนยันทฤษฎีที่อธิบายคุณสมบัติทางกายภาพของวัสดุหลายชนิด ยกตัวอย่างเช่นคุณสมบัติที่น่าสนใจของโลหะนิเกิล นั่นคือธรรมชาติที่ดูเหมือนว่าค้านกันระหว่างคุณสมบัติการนำไฟฟ้าและคุณสมบัติทางแม่เหล็ก ซึ่งเป็นเรื่องที่ศึกษาในงานวิทยานิพนธ์นี้ คุณสมบัติดังกล่าวสามารถอธิบายได้โดยการทดลองด้านโฟโตอิมิชชัน จากการทดลองมีการพบ 3d-4s hybridization และความหนาแน่นที่สูงของแถบพลังงาน 3d ในนิเกิล การเกิดการ hybridization ดังกล่าวนั่นส่งผลให้ holes ในระดับชั้นพลังงาน 3d มีส่วนร่วมในการนำไฟฟ้า และการที่แถบพลังงาน 3d มีความหนาแน่นที่สูงนั้นทำให้มวลของ hole กล่าวมีค่าที่สูงมาก การค้นพบดังกล่าวยืนยันทฤษฎีที่อธิบายคุณสมบัติการนำไฟฟ้าที่แย่ของโลหะนิเกิล นอกจากนั้นการทดลองทางด้านโฟโตอิมิชชันที่นำสปินของโฟโตอิเล็กตรอนและโพลาไรเซชันมาพิจารณาแสดงให้เห็นว่าสนามเชิงโมเลกุลมีจริง ซึ่งสนามดังกล่าวเป็นสาระทางทฤษฎีที่สำคัญมากเกี่ยวกับ ferromagnetism ในวิทยานิพนธ์นี้ยังมีการพิจารณาและให้เหตุผลของความแตกต่างระหว่างผลที่ได้จากการทดลองและผลทางทฤษฎี

สาขาวิชา ฟิสิกส์
ปีการศึกษา 2542

ลายมือชื่อนักศึกษา
ลายมือชื่ออาจารย์ที่ปรึกษา
ลายมือชื่ออาจารย์ที่ปรึกษาร่วม
ลายมือชื่ออาจารย์ที่ปรึกษาร่วม

MR. JIANG YANG: PHOTOEMISSION STUDIES OF METALLIC NICKEL THESIS ADVISOR: PROF. TAKEHIKO ISHII, Ph.D. 81 PP.
ISBN 974-7359-49-9

Photoemission experiments have been used to verify theoretical explanation for physical properties of many materials. For example, interesting properties of metallic nickel, i.e. seemingly contradictory nature between electrical conduction and magnetism, which is studied in this thesis work, could be explained by photoemission experiments. Through photoemission experiments, the 3d-4s hybridization and very high density of 3d states can be demonstrated clearly. The hybridization results in the contribution of 3d holes to electrical conductivity, and the high density of state gives rise to a very high effective mass. These findings verify theoretical explanation for poor electrical conductivity of metallic nickel. In addition, spin-polarized photoemission shows the existence of molecular field, which is the theoretical essence for ferromagnetism. The discrepancies between experimental and theoretical results are also discussed in this thesis.

สาขาวิชา ฟิสิกส์
ปีการศึกษา 2542

ลายมือชื่อนักศึกษา
ลายมือชื่ออาจารย์ที่ปรึกษา
ลายมือชื่ออาจารย์ที่ปรึกษาร่วม
ลายมือชื่ออาจารย์ที่ปรึกษาร่วม

Acknowledgment

First I would like to express my sincere thanks to my supervisor, Prof. Dr. Takehiko Ishii. Without his long-term guidance and patient help, this thesis would not be possible.

I also like to express my gratitude to all the teachers who taught and helped me during I studied in the School of Physics of Suranaree University of Technology. They are Prof. Dr. Edouard B. Manoukian, Dr. Yupeng Yan, Dr. Prayoon Songsiriritthigul and Dr. Chinorat Kobdaj.

Finally, I wish to express my especial thanks to the chairman of School of Physics of Suranaree University of Technology, Assoc. Prof. Dr. Prasart Suebka, for his long-term and warmhearted support, encouragement and help.

Jiang Yang

Contents

Page

Contents (continued)

List of Tables

Table **Page**

List of Figures

Figure **Page**

List of Figures (continued)

Chapter I

Introduction

Understanding of the electromagnetic properties of metals is quite important for finding novel ways to utilize them. Among various metals, nickel has quite interesting characters regarding electrical conductivity and magnetism. On the one hand it is not such a good conductor as a simple metal. This suggests that the number of itinerant electrons as energy-band electrons is not large or the mobility of conduction electrons is small. On the other hand the localized spins are supposed to bring about its ferromagnetism below a rather high Curie temperature. Thus, metallic nickel appears to present a good example for understanding the cause of seemingly contradictory nature as electrical conduction versus magnetism. In a simple mind, the interesting characters of nickel seem to be caused by the partially filled 3d band. We should know the electronic structure in order to clarify such nature of nickel. This kind of study also helps understanding the properties of other interesting materials which show more sophisticated phenomena.

A number of different experimental techniques can be used to obtain information about the electronic structure of materials, including the distribution of states as a function of energy (the density of states) and of crystal momentum (band structure). Many of these techniques are optical in nature: We utilize the interaction between photons and electrons system. In addition, by measuring the number of electrons generated by the photoelectric effect (photoemission) as a function of emission angle, the electronic band structure, $\varepsilon(\mathbf{k})$, can be traced out experimentally. So far, a large number of experimental and theoretical investigations of the electronic structure of nickel have been reported. Many of them are related, directly or indirectly, with photoemission phenomena. In the present thesis, an overview of the existing photoemission data on nickel is perform.

1.1 Photoemission Spectroscopy

Photoemission, the emission of electrons from a material caused by absorption of photons, was discovered by Hertz (1887) in the study of the electromagnetic waves. In the following years, the phenomena associated with this effect had puzzled people till Einstein explained the threshold energy of emitted photoelectrons found in metals by the quantum nature of light. The distinctive energy relation giving the maximum kinetic energy of a photoelectron excited with fixed photon energy is given as

$$\varepsilon_{\max} = \hbar\omega - e\varphi \,. \qquad (1.1)$$

Where $\varepsilon_{\max}$, $\hbar\omega$ and $e\varphi$ are the maximum kinetic energy of photoelectrons, the photon energy and the work function of an emitting solid.

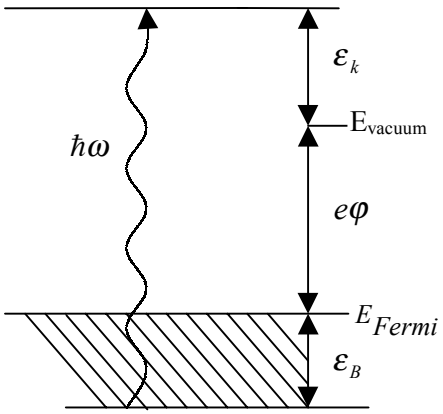

Photoemission

Figure 1.1. Energy diagram for photoemission (photon in, electron out) (Himpesl, F.J. 1995)

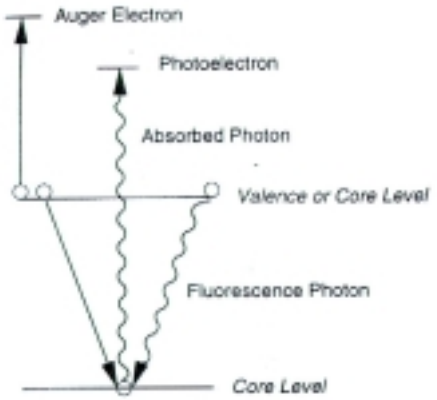

Figure 1.2. Energy diagram for core-level photoemission. The core-hole decays by the Auger process (left) or by the fluorescence emission (right) (Himpesl, F.J. 1995)

In the initial state of photoemission, there is a solid in the ground state with an energy E_g with **N** electrons and a photon with an energy of $\hbar\omega$. In the final state of

photoemission, there is a solid system with a different energy E_f. In this final state, there is the solid of $(\mathbf{N}-1)$ electrons with total energy $E_f(N-1)$ and a photoelectron with energy ε_u in the solid. The energy conservation principle restricts the relevant energies as

$$\begin{aligned} E_g + \hbar\omega &= E_f \\ &= E_f(N-1) + \varepsilon_u \end{aligned} \qquad (1.2)$$

If the photoelectron comes out of the solid , the kinetic energy ε_k of the photoelectron measured outside the solid is given as

$$\varepsilon_k = \varepsilon_u - e\varphi, \qquad (1.3)$$

where $e\varphi$ is the work function of the solid. Here we implicitly assigned the zero energy level to be at the vacuum level. The relation (1.3) indicates that the photoelectron loses its kinetic energy by an amount $e\varphi$ when it leaves the solid. This is caused by the retardation of photoelectrons by the ionized solid. In a different viewpoint, it is understood that the kinetic energy of a photoelectron outside the solid is zero at the vacuum level. This situation is dependent on the method of the measurements. If the sample is grounded, the zero potential level is at the vacuum level. If a retardation voltage, V_r, is applied to the sample, the vacuum level is pulled down below the zero potential level by an amount equal to eV_r. In any cases, the Fermi level is located below the vacuum level by an amount $e\varphi$.

We define the binding energy of the emitted electron as

$$\varepsilon_B \equiv E_f(N-1) - E_g. \qquad (1.4)$$

From (1.2), (1.3) and (1.4), we have

$$\varepsilon_B = \hbar\omega - \varepsilon_k - e\varphi \qquad (1.5)$$

The relation shown in equation (1.2) through (1.5) is illustrated in Fig.1.1. The figure is self-explaining.

There are other electron- and photon-emission phenomena related to photoemission. They are shown schematically in Fig. 1.2. When an electron is excited from the core level to the conduction state, a hole is left in the core level. Then, it is possible that a valence or outer-core-level electron fills the hole level and an electron in the valence or outer core level is excited. The energy conservation is satisfied in this process and it is called the Auger process (left). It is also possible that the fluorescence (right) process occurs instead of the Auger process.

The process of photoemission can be explained by the three-step model, which is extremely useful to interpret photoemission experiments. In the first step, an electron in a solid is excited by absorbing incident photons. In the second step, the photoexcited electron travels through the sample to the surface with or without the secondary electrons generated by electron-electron inelastic scattering. Finally, in the third step, the photoelectron escapes through the surface into the vacuum where it is detected. Fig.1.3 shows the three-step process.

The advance in the ultra-high vacuum (UHV) technique has greatly promoted the development of photoemission spectroscopy (PES). It is because the photoemission process is quite surface-sensitive. We know a photoelectron can lose energy by creating electron-hole pairs or plasmons during its escape. These processes actually limit the escape depth. The escape depth is defined as the mean free path, λ, of photoelectrons reaching the surface without being scattered. In general, the escape depth is only of the order of a few Angstrom. The escape depth of the electrons is mainly determined by electron-electron collisions. The inverse escape depth λ^{-1} is described by the mean free electron-electron distance r_s, which is roughly equal for all materials, and Lbach, H. (1977) obtained

$$\lambda^{-1} \cong \sqrt{3}\frac{a_0 R}{\varepsilon_{kin}} r_0^{-3/2} \ln[(\frac{4}{9\pi})^{2/3}\frac{\varepsilon_{kin}}{R} r_s^2], \qquad (1.6)$$

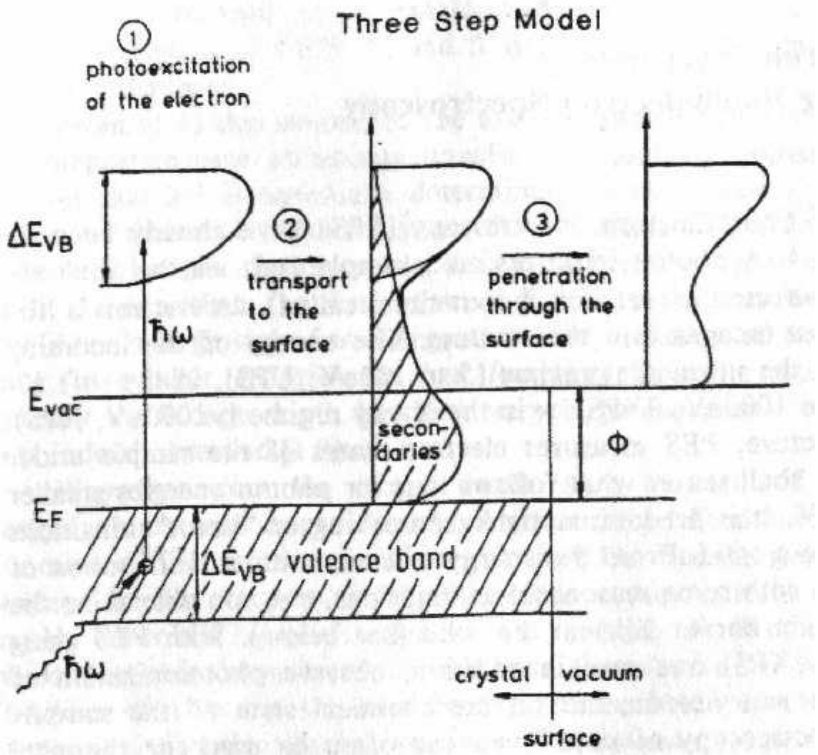

Figure1.3 Photoemission spectra as illustrated in terms of the three-step process 1) photoexcitation of an electrons; 2) travel to the surface with concomitant production of secondaries (shaded); 3) penetration through the surface (barrier) and escape into the vacuum (Hufner, S. 1996)

where $a_0 = 0.529A$, $R = 13.6eV$ and r_s is measured in units of the Bohr-radius a_0. Therefore, almost all materials show a similar energy dependence of the mean electron escape depth. This means that any spectroscopy of the solid surface involving only the electrons from a very thin layer of the sample. Thus, if one wishes to study the bulk properties of the solid, one has to work with atomically clean surface. Investigations of surface states or adsorbed molecules require UHV conditions to prevent interference from adsorbed contaminants.

In PES, for different research purposes, excitation light with different energies is adopted. In the ultraviolet photoemission spectrocopy regime ($h\omega \cong 5$eV to 100eV, UPS), it is predominatly $\mathbf{k}$-conserving or "direct" transitions that are excited in a solid. Here $\mathbf{k}$ is the electron wave vector and $\hbar\mathbf{k}$ is equal to the crystal momentum of the electron. From the energy and momentum distribution of the electrons, and with

some reasonable assumptions, one can determine the electronic dispersion curves $\varepsilon(\mathbf{k})$ in the solid. In the X-ray photoemission spectroscopy regime ($\hbar\omega \geq 1000$eV, XPS), one can observe photoionization of core levels. Their energies depend on the chemical state of the sample. During the last two decades, synchrotron radiation has emerged as a powerful and convenient excitation source in photoemission experiments. It has a number of desirable properties as:

1. A continuous spectral distribution from the infrared region into the X-ray region;
2. High intensity;
3. A high degree of polarization (completely linearly polarized in the plane of orbital and elliptically out of the plane);
4. A pulsed time structure given by the orbital frequency of the circulating electron bunch.

The use of synchrotron radiation in photoemission experiments enhanced the range of observation considerably. For instance, the continuous spectrum enabled the continuous change in the excitation energy. Thus, we can carry out the resonant photoemission measurements. The tunability of excitation energy also makes it possible to carry out the normal emission angle-resolved photoemission measurements. By scanning excitation energies, the energy band mapping is achievable. The polarization nature is used to sort out the transitions through the polarization selection rule. The soft x-ray region is exploited by using synchrotron radiation.

It is interesting to know what kind of information can be gained by this technique. In principle, the hamiltonian, H^{int}, for the interaction between electrons and electromagnetic radiation with the vector potential $\mathbf{A}$ can be written as

$$H^{\text{int}} = \frac{1}{2mc}(\mathbf{A}\cdot\mathbf{P} + \mathbf{P}\cdot\mathbf{A}) \qquad (1.7)$$

where $\mathbf{P}$ is the momentum operator of an electron. Let E_f and E_g denote the energies of the final states $|f\rangle$ and the initial states $|i\rangle$, respectively. The transition probability between initial and final states is given by Fermi's Golden Rule as

$$w_{fg} = \frac{2\pi}{\hbar}\left|\langle f,u\left|H^{\text{int}}\right|g\rangle\right|^2 \delta(E_f - E_g - \hbar\omega)\,. \qquad (1.8)$$

For convenience, the transition matrix element is written as M_{fg}

$$M_{fg}(\varepsilon_k,\hbar\omega) = \langle f\left|H^{\text{int}}\right|g\rangle \qquad (1.9)$$

Assuming that the matrix element M_{fg} does not vary much with $\hbar\omega$ and ε_k and can be replaced with its average value, $\widehat{M}_{fg}$, at fixed $\hbar\omega$ one obtain the intensity of photoelectrons as

$$N(\varepsilon,\hbar\omega) \propto \left|\widehat{M}_{fg}\right|^2 \sum \delta(E_f - E_g - \hbar\omega)\delta(\varepsilon - \varepsilon_u) \qquad (1.10)$$

Here, we define initial one-electron energy as

$$E_g = E_g(N-1) + \varepsilon_i \qquad (1.11)$$

where $E_g(N-1)$ is the total energy of the $(N-1)$ electrons except the i-th electron in the ground state and ε_i is the energy of the i-th electron.

Using (1.2) and (1.11), we can rewrite the photoelectron intensity distribution as

$$\begin{aligned} N(\varepsilon,\hbar\omega) &\propto \left|\widehat{M}_{fg}\right|^2 \sum \delta(E_f - E_g - \hbar\omega)\delta(\varepsilon + E_f(N-1) - E_f) \\ &= \left|\widehat{M}_{fg}\right|^2 \sum \delta(\varepsilon + E_f(N-1) - E_g - \hbar\omega) \qquad (1.12) \\ &= \left|\widehat{M}_{fg}\right|^2 \sum \delta(\varepsilon - \varepsilon_i - \hbar\omega + (E_f(N-1) - E_g(N-1)) \end{aligned}$$

The energy, $E_R(N-1)$, defined as

$$E_R(N-1) = E_f(N-1) - E_g(N-1) \tag{1.13}$$

is called the relaxation energy. If the relaxation energy is small, (1.12) is proportional to the one electron density of states defined as

$$D(\varepsilon) = \sum \delta(\varepsilon - \varepsilon_i) \tag{1.14}$$

The function, $D_N(\varepsilon)$, defined as

$$D_N(\varepsilon) = \sum \left|\langle f|T|g\rangle\right|^2 \delta(E_f - E_g - \hbar\omega)\delta(\varepsilon - \varepsilon_u) \tag{1.15}$$

is called the optical density of states. The first factor in the summation will be explained later. The optical density of states given in (1.15) is nothing but the photoelectron intensity distribution $N(\varepsilon_k, \hbar\omega)$ or $N(\varepsilon_B, \hbar\omega)$ that is called the energy distribution curve if it is illustrated as a function of ε_k or ε_B.

The argument described above indicates that the distribution of photoemitted electrons is approximately proportional to the density of states (DOS) in a simplified picture. Thus, we measure a density of states, or rigorously the optical density of states, in the photoemission experiments. If electrons with different angular momentum are involved, the spectrum includes the contributions from the various angular momentum states with different strengths, because M_{fg} depends on the angular momentum of the initial state.

We should remark that the expression of transition matrix element M_{fg} is a special from of a more general expression. In the general case, the transition matrix element is given by

$$T_{f,g} = \langle f|T|g\rangle \tag{1.16}$$

where the T is transition operator and defined as

$$T = V_T + V_T \frac{1}{\hbar\omega + E_g - H_0 - V_T + i0^+} V_T \qquad (1.17)$$

Here V_T is the perturbation operator, H_0 is the quantized hamiltonian of the electron system without the perturbation terms causing the electronic transition and 0^+ is a positive infinitesimal. We can obtain the T matrix by solving Lippman-Schwinger equation or solving *Schrödinger* equation formally using the one-particle Green function.

Not only the direct electron-photon interaction H^{int} but also the Auger interaction V_A contribute to the perturbation. Because the Auger matrix element is much larger than that of the dipole matrix element for the optical transition in some cases, it is reasonable to retain H^{int} only to the first order and leave V_A to the infinite order, then we have

$$T = H^{\text{int}} + V_A \frac{1}{\hbar\omega + E_g - H_0 - V_A + i0^+} H^{\text{int}} \qquad (1.18)$$

In the case where the resonant excitation is predominant, the relaxation of the intermediate excited states is incomplete.

One of the successful applications of photoemission is the study for metallic nickel. In the present thesis, we will see the good agreement between experimental results and theories. More details about photoemission spectroscopy will be given in the next two chapters.

Chapter II

Photoemission Spectroscopy and Electrical Conductivity of Metallic Nickel

In solid physics, people regard that the metallic bonds hold the metallic atoms together to be metal. Metals are characterized by high electrical conductivity, and a large number of electrons in a metal are free to move about. The electrons available to move about are called conduction electrons which are from the valence electrons of the atoms. The metallic bond is just the electrostatic force between the free electrons pool and the ions. So, metals usually adopt close-packed structures. For example, the cubic close-packed (face-centered cubic, f.c.c.) arrangement occurs in metallic nickel.

2.1 Energy Band Theory

In classical theory of metals, the properties of metals could be explained by their valence electrons. Valence electrons were considered to behave within a metal in a way corresponding to gas molecules in a container, obeying the same laws. This implies that the electrons are free, have a continuous energy distribution and can be described by the classical, Maxwell- Boltzmann statistics. But it provides an incorrect temperature dependence of the electrical resistivity and the heat capacity. The disparity between the heat capacity and the electrical resistivity reveals an inherent inconsistency in this theory. In quantum mechanics not every value of the energy is allowed, and the continuous distribution of energies is replaced by a discrete set of allowed energy levels. The energy distribution at a finite temperature is given by Fermi-Dirac statistical mechanics.

First, let us consider the valence electrons in a metal. For convenience, we suppose that the electrons are confined to a cube of edge inter-distance L and the potential tends to infinity. The *Schrödinger* equation for a free electron in three dimensions is

$$-\frac{\hbar^2}{2m}\nabla^2\Psi(x,y,z)=E\Psi(x,y,z) \tag{2.1}$$

Obviously, the differential equation (2.1) is separable. Thus, we separate variables to get

$$\Psi(x,y,z)=\boldsymbol{j}_1(x)\boldsymbol{j}_2(y)\boldsymbol{j}_3(z) \tag{2.2}$$

Substituting (2.2) into (2.1), we find that *Schrödinger* equation (2.1) is written into

$$\begin{cases}\dfrac{d^2\boldsymbol{j}_1(x)}{dx^2}+k_x^2\boldsymbol{j}_1(x)=0\\ \dfrac{d^2\boldsymbol{j}_2(y)}{dy^2}+k_y^2\boldsymbol{j}_2(y)=0\\ \dfrac{d^2\boldsymbol{j}_3(z)}{dz^2}+k_z^2\boldsymbol{j}_3(z)=0\end{cases} \tag{2.3}$$

if the following conditions are satisfied:

$$E=\frac{\hbar^2}{2m}(k_x^2+k_y^2+k_z^2)\,. \tag{2.4}$$

For convenience, we define $\mathbf{k}$ as follows:

$$E=\frac{\hbar^2\mathbf{k}^2}{2m}=\frac{\hbar^2}{2m}(k_x^2+k_y^2+k_z^2)\,. \tag{2.5}$$

The solutions of (2.3) are given as

$$\begin{cases} \boldsymbol{j}_1(x) = A_x e^{ik_x x} + B_x e^{-ik_x x} \\ \boldsymbol{j}_2(x) = A_y e^{ik_y y} + B_y e^{-ik_y y} \\ \boldsymbol{j}_3(x) = A_z e^{ik_z z} + B_z e^{-ik_z z} \end{cases} \tag{2.6}$$

where A_a and B_a ($\boldsymbol{a} = x, y, z$) are constants to be determined by the boundary conditions. We set up a realistic boundary condition known as the box normalization. According to it, solutions should satisfy the boundary conditions: at $x = 0$ and $x = L$,

$$\begin{cases} \boldsymbol{j}_1 = 0 \\ \boldsymbol{j}_2 = 0 \\ \boldsymbol{j}_3 = 0 \end{cases} \tag{2.7}$$

L is the length of the solid cube. Then we obtain

$$A = -B \tag{2.8}$$

and

$$\begin{cases} \sin k_x L = 0 \\ \sin k_y L = 0 \\ \sin k_z L = 0 \end{cases} \tag{2.9}$$

From (2.9), k_a should satisfy the following conditions:

$$\begin{cases} k_x = \dfrac{n_x \boldsymbol{p}}{L} \\ k_y = \dfrac{n_y \boldsymbol{p}}{L} \\ k_z = \dfrac{n_z \boldsymbol{p}}{L} \end{cases}. \tag{2.10}$$

where the n_x, n_y, n_z are integers. So, the eigenfunction of an electron is

$$\Psi = C \sin k_x x \sin k_y y \sin k_z z . \qquad (2.11)$$

Where C is normalization constant.

The energy of electron is

$$E = \frac{h^2}{8mL^2}(n_x^2 + n_y^2 + n_z^2) . \qquad (2.12)$$

As a result of the translational symmetry of a crystal, the eigenfunction should satisfy the periodic boundary condition as

$$\boldsymbol{j}_a(\boldsymbol{a} + a) = \boldsymbol{j}_a(\boldsymbol{a}) . \qquad (2.13)$$

Where a is the lattice constant. By the repeated applications of the condition, (2.13), we have

$$\boldsymbol{j}_a(\boldsymbol{a} + Na) = \boldsymbol{j}_a(\boldsymbol{a}) \qquad (2.14)$$

If N atoms exist in the $\boldsymbol{a}$ direction of the cube, L is equal to Na.

The condition (2.14) is satisfied, if the following relations hold:

$$\begin{cases} \sin k_a Na = 0 \\ \cos k_a Na = 1 \end{cases} \qquad (2.15)$$

Thus we have

$$k_a = \frac{2\boldsymbol{p} n_a}{Na} = \frac{\boldsymbol{p}}{a}\left(\frac{n_a}{N/2}\right) \qquad (2.16)$$

$$n_a = -\frac{N}{2}, -\frac{N}{2}+1, \cdots\cdots, 0, \cdots\cdots, \frac{N}{2}-1, \frac{N}{2} \qquad (2.17)$$

(2.16) and (2.10) are equivalent to each other, if we take the values of n_a in (2.10) as

$$n_a = 0, 1, 2, \cdots\cdots, N$$

or

$$n_a = 0, -1, -2, \cdots\cdots, -N$$

In this case, (2.10) is written as

$$k_a = \frac{p}{a}(\frac{a}{N}) \qquad (2.18)$$

Since we take both positive and negative values of k, e^{ika} and e^{-ika} are equivalent. Thus we take only $+k$ term in (2.6) as the eigenfunctions without losing generality, namely,

$$\Psi = Ae^{i\mathbf{k}r}. \qquad (2.19)$$

Here, A is the normalization constant.

It is clear, that the wave function represents a running plane wave. If we define the momentum as $\mathbf{p} = \hbar\mathbf{k}$, the relation between the kinetic energy and the momentum is satisfied. Note that we are dealing with a nearly free electron and the potential is almost zero, since n_a is an integer. It is obvious that $\Delta n_a = 1$, then we have

$$\Delta k = (\frac{2p}{a})\frac{1}{N} \qquad (2.20)$$

Because N is a very large number of the order of 10^{23}, Δk is very small and k is practically continuous.

In the ground state of a system of N free electrons the occupied orbits may be represented as point inside a sphere in $\mathbf{k}$ space and we should note that the energy is

equal if $|\mathbf{k}|$ is equal. The energy at the surface of the sphere is the Fermi energy; the wave vectors at the Fermi surface have a magnitude k_F such that

$$E_F = \frac{\hbar^2}{2m} k_F^2 \ . \qquad (2.21)$$

If n_a changes by Δn_a, corresponding k_a changes by $\frac{2\pi}{a}\frac{\Delta n_a}{N}$. If the number of the points in the k space is changed by $\Delta n_x \cdot \Delta n_y \cdot \Delta n_z$, the corresponding volume in the k space is changed by

$$|\Delta k|^2 = \frac{(2\pi)^3}{(Na)^3} = \frac{(2\pi)^3}{V} \qquad (2.22)$$

The Fermi sphere has volume $4\pi k_F^3/3$, then, the total number of orbits in this sphere is

$$N = 2 \cdot \frac{V}{(2\pi)^3}\frac{4\pi k_F^3}{3} = \frac{V}{3\pi^2} k_F^3 \ . \qquad (2.23)$$

Here the factor 2 is from the spin degeneracy.

One point in the k space corresponds to one state. The total number of states up to the values of the momentum, k is given as

$$N_k = \frac{V}{3\pi^2} k^3 = \frac{V}{3\pi^2} \cdot (\frac{2m}{\hbar^2})^{3/2} E^{3/2} \qquad (2.24)$$

By the definition of density of states, the number of states, $D(E)$, per unit energy range is

$$D(E) = \frac{dN}{dE} = \frac{V}{2\pi^2}\left(\frac{2m}{\hbar^2}\right)^{3/2} E^{1/2} = const \times E^{1/2} \qquad (2.25)$$

Fig 2.1 shows the relation between $D(E)$ and E. In the figure, two cases are shown. One is that for zero temperature, the other is that for a finite temperature T. At finite temperature, the Fermi-Dirac distribution function $f(E,T)$ is multiplied,

$$f(E,T) = \frac{1}{1+e^{(E-E_F)/k_B T}} \qquad (2.26)$$

Here k_B is the Boltzmann constant. At zero temperature, the states below the Fermi level are completely occupied, since $f(E,0) = 0$. Ata a finite temperature, the states near and above the Fermi level are partially occupied and the state near and below the Fermi level are partially unoccupied. The energy range where this occurs is confined to

$$\Delta E \approx k_B T$$

The free electron gas model has been considered the electrons within the metal are in a constant internal potential. It is equivalent to the case that the constant potential is zero. However, the potential within a metallic lattice is not constant.

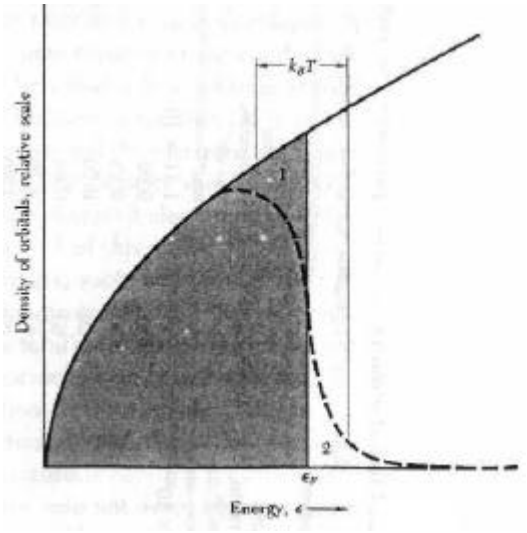

Figure 2.1 Density of nearly-free electron states as a function of the energy in three dimensions. The dashed curve represents the density $f(E,T)D(E)$ of filled orbitals at a finite temperature ($f(E,T)$ denotes the Fermi-Dirac distribution function), k_BT is small in comparison with E_F. The shaded area represents the filled energy states at zero temperature. (Kittle, C. 1986 pp.133)

As used already the one electron potential in a crystal has the translational symmetry, as

$$V(r+a)=V(r) \tag{2.27}$$

The *Schrödinger* equation reads

$$[-\frac{\hbar^2}{2m}\nabla_r^2+V(r)]\Psi(r)=E\Psi(r) \tag{2.28}$$

If the potential satisfies the translational symmetry condition as (2.27), the Floque theorem and the Bloch theorem tell us that the solution of (2.28) has the form

$$\Psi(r)=Ae^{i\mathbf{k}r}u_{jk}(\mathbf{k}) \tag{2.29}$$

Here $\mathbf{k}$ is similar to k_a showing up in the free electron approximation described earlier. More definitely it has the form.

$$\mathbf{k}=k_1\mathbf{b_1}+k_2\mathbf{b_2}+k_3\mathbf{b_3} \tag{2.30}$$

$$k_i=\frac{2pn_i}{L_i} \qquad (i=1,\ 2,\ 3) \tag{2.31}$$

$$\begin{cases}\mathbf{b_1}=\dfrac{\mathbf{a_2}\times\mathbf{a_3}}{\mathbf{a_1}\cdot(\mathbf{a_2}\times\mathbf{a_3})}\\ \mathbf{b_2}=\dfrac{\mathbf{a_3}\times\mathbf{a_1}}{\mathbf{a_2}\cdot(\mathbf{a_3}\times\mathbf{a_1})}\\ \mathbf{b_3}=\dfrac{\mathbf{a_1}\times\mathbf{a_2}}{\mathbf{a_3}\cdot(\mathbf{a_1}\times\mathbf{a_2})}\end{cases} \tag{2.32}$$

Here $\mathbf{a_1}, \mathbf{a_2}, \mathbf{a_3}$ are the unit vectors of the crystal lattice; $\mathbf{b_1}, \mathbf{b_2}$ and $\mathbf{b_3}$ are the unit vectors in the reciprocal lattice. A general reciprocal lattice vector is defined as

$$\mathbf{G_n} = 2\pi(n_1\mathbf{b_1} + n_2\mathbf{b_2} + n_3\mathbf{b_3})$$

The function given by (2.29) is called the Bloch function. The eigen energy is a function of $\mathbf{k}$, as

$$E = E_j(\mathbf{k}) \qquad (2.33)$$

It is shown that E is a periodic function of k and satisfies the periodic boundary condition in the reciprocal lattice as

$$E_j(\mathbf{k}) = E_j(\mathbf{k} + \mathbf{G_n}) \qquad (2.34)$$

If we compare (2.31) with (2.16) or (2.18), we see $\mathbf{k}$ changes almost continuously.

The energy as a function of $\mathbf{k}$ is called the energy band, since the energy of an electron in the periodic lattice seeing the one electron potential has a width determined by the dependence of E on $\mathbf{k}$. The finite range of the energy appears since $E(\mathbf{k})$ is a periodic function of $\mathbf{k}$.

The region in the $\mathbf{k}$ space defined as

$$\begin{cases} -\dfrac{\pi}{a_1} \le k_1 \le \dfrac{\pi}{a_1} \\ -\dfrac{\pi}{a_2} \le k_2 \le \dfrac{\pi}{a_2} \\ -\dfrac{\pi}{a_3} \le k_3 \le \dfrac{\pi}{a_3} \end{cases} \qquad (2.35)$$

is called the first Brillouin zone or just the Brillouin zone. The energy band and the Bloch function have the periodicity of $\mathbf{G_n}$ defining the Brillouin zone. Because of this periodicity, the energy bands can be reduced into the first Brillouin zone. The band gaps are illustrated in Fig. 2.2

The density of states in the energy band picture is given as

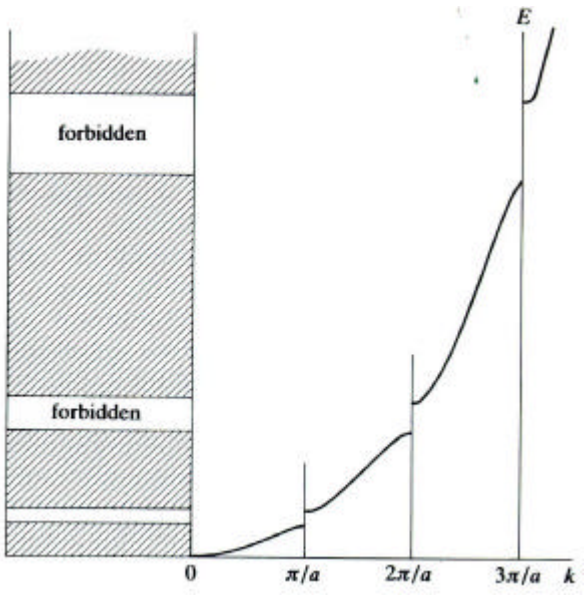

Figure2.2 Diagram of the energy band. Note that the higher the energy of the band the large its width in energy. (Myers, H.P. 1997)

$$D(E) = \frac{\partial N}{\partial E} = \frac{2V}{(2\pi)^3} \iint \int_E^{E+dE} dk^3 = \frac{2V}{(2\pi)^3} \iint \frac{dS}{\left| grad_k E(k) \right|} \tag{2.36}$$

where the integration is to be carried out on the equi-energy surface in the Brillouin zone. By a simple calculation, we can show that an energy band splits into two energy levels at the zone boundary where k_i equals to $\pm \frac{\pi}{a_i}$. The energy separation there is called the band gap.

One can distinguish insulator and metal from their band structure. If the valence electrons exactly fill one or more bands, leaving others empty, the crystal will be an insulator. If a crystal has an even number of valence electrons per primitive cell, it is necessary to consider whether or not the bands overlap in energy. If they do so, then instead of one filled band giving an insulator, we can have two partly filled bands giving a metal as shown in Fig 2.3.

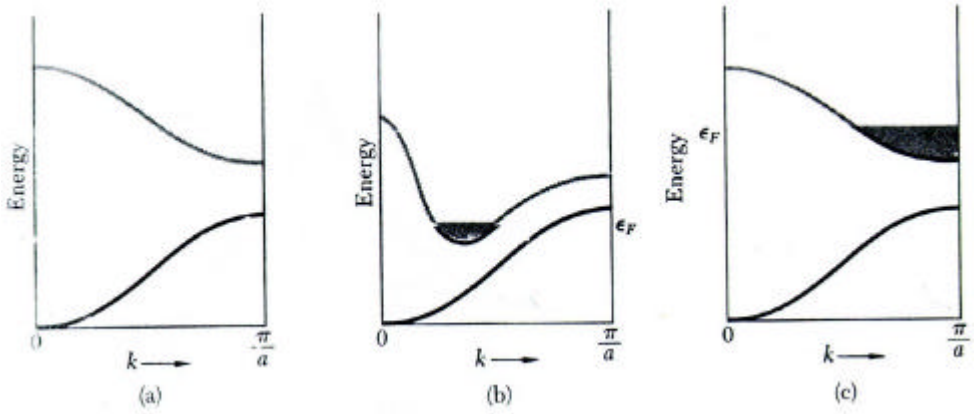

Figure2.3 Occupied states and band structures giving (a) an insulator (b) a metal or a semimetal because of band overlap and (c) a metal because of electron concentration. The illustration is made for the reduce zone. (Kittle, C. 1986 pp.178)

In the case of Ni, the 3d band is not completely filled, it is a rather narrow band, since d-electron wavefunction do not spread so far out as s-electron functions, and interactions between d electrons on adjacent atoms are smaller than those between s electrons. The narrow 3d band is overlaped by the broad 4s band, and the 3d band gives a high magnitude of density of states $D(E)$ as shown in Fig 2.4.

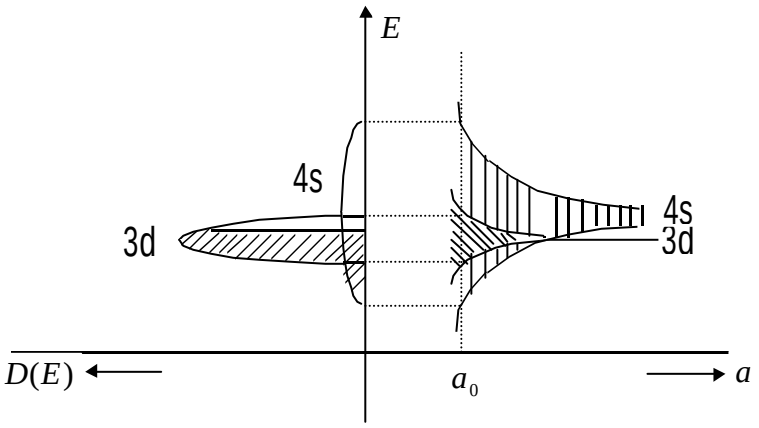

Figure 2.4 Energy bands of nickel. To the right is shown the bandwidth of 4s and 3d states as functions of interatomic distance a (a_0 is the value for solid nickel). To the left is shown $D(E)$, the shaded area indicating the filled parts of the bands. (Bleaney, B.I. 1992)

2.2 Electric Conductivity

It's well known that metals have electrical resistivity. In perfect crystals, the motion of electrons is in perfectly periodic lattices, which can be expressed by the Fourier transform of Bloch function

$$\Psi(r) = e^{i\mathbf{k}\cdot r} u_{jk}(\mathbf{k}) \qquad (2.37)$$

There is no damping term and the wave function does not decay. But in practical crystals, the impurity, defect, imperfection and phonon will distort the periodic potential and interact with the conduction electrons to prevent the free motion.

The equation of motion experienced by a free electron subject to applied electric and magnetic field is

$$F = m_e \frac{dv}{dt} = -e(E + v \times B) \qquad (2.38)$$

where the velocity, v, is identified with the group velocity of the wave packet namely:

$$v_g = \nabla_k \boldsymbol{w}(k) = (1/\hbar)\nabla_k E(k) \qquad (2.39)$$

here k, $E(k)$ and $\boldsymbol{w}(k)$ are wave vector, electron energy and frequency, respectively. In considering the electrical conductivity, the magnetic field is assumed to be zero. Because of the existence of scattering, the electrons can not be accelerated without limit. These scattering events cause a reversal in the electron momentum and hence act like a damping force in the equation of motion. If it is assumed that, at every scattering event, the extra drift velocity v_d $(= (v - v_{th})$, where v_{th} is the equilibrium thermal velocity) imparted by the electric field, is removed on average, with $\boldsymbol{t}$ being

the average time between electron collisions, then the equation of motion can be modified by the addition of a damping term, $m_e v_d / \tau$,

$$m_e(\frac{dv}{dt} + \frac{v_d}{\tau}) = -e(E + v \times B) \qquad (2.40)$$

The quantity τ is also called the electron relaxation time. This situation can be described as follows: First an electron is moving in the crystal with velocity equal to its equilibrium speed, the thermal velocity. Under the action of the electric field, the electron is accelerated toward the applied electric field and its velocity increases. After a period of τ , the electron is scattered and loses its velocity gained by the acceleration due to the applied field. The amount of the loss in the velocity is proportional to that of the gained velocity, the drift velocity. The probability that this velocity loss occur is $1/\tau$.

In zero field, the mean thermal electron velocity $\bar{v}$ associated with the equilibrium Fermi-Dirac distribution must be zero. However, when an electric field is applied, there is a finite drift velocity v_d . At the equilibrium state, dv/dt =0. Then we obtain for the $B = 0$ case

$$v_d = -\frac{e\tau}{m_e} E \qquad (2.41)$$

The electrical current density is $j = -env.$ Where n is the electron density, thus, the d.c conductivity σ can be written as

$$\sigma = \frac{ne^2\tau}{m_e} \qquad (2.42)$$

where the m_e is effective mass. The effective mass appears because the motion of electrons in solid is in a periodic potential. An electron in a crystal can not strictly be

treated in isolation (it forms a system jointly with the lattice), the momentum of such an electron is not a true momentum, but a crystal momentum and, as such, momentum may be transferred freely between electron and lattice. The effective mass is defined by

$$m^* = \hbar^2 \Big/ \frac{d^2E}{dk^2} \propto \left(\frac{d^2E}{dk^2} \right)^{-1}. \qquad (2.43)$$

Thus, clearly, the electric resistivity is depended on the relaxation time and effective mass which are determined by electronic structure of a particular material. Now, let's look into photoemission experiment, the useful means to obtain the information of electronic structure or band structure. (Daniel D.Pollack 1990,1993 and Elliott, S. 1996)

2.3 Theories of Photoemission Spectroscopy

We have presented the theoretical formulae describing the photoemission spectra. In what follows we will discuss the electronic states of Ni in relation to the energy band nature and the deviation from it. Thus, we start with modifying the general formulae given in (1.15) to be adequate for the energy band state. Since we will deal with the one electron state, we naturally assume that the relaxation energy, $E_R(N-1)$, is small. Then we look into the transition matrix element part. First we assume that the final state eigen function and the initial state eigen function are given as

$$|\Psi_f> = |m>|\Psi_f(N-1)> \qquad (2.44)$$

$$|\Psi_g> = |i>|\Psi_g(N-1)> \qquad (2.45)$$

Here $|m>$ denote the state of a photoelectron with a kinetic energy ε_m inside a solid and $|i>$ denotes the state of an electron in the ground state with an energy ε_i. For

simplicity, we ignore the Auger operator V_A in the T matrix. Taking into account the fact that the electron-photon operator H^{int} consists of the linear combination of one-electron operator $\mathbf{p}$, the transition matrix element is written as

$$\begin{aligned} <\Psi_f \mid T \mid \Psi_g> &= <\Psi_f \mid \mathbf{Ap} \mid \Psi_g> \\ &= <\Psi_f(N-1) \mid \Psi_g(N-1)> \cdot <m \mid p_e \mid i> \end{aligned} \tag{2.46}$$

Here we defined the operator p_e, as

$$p_e = \mathbf{AP} \tag{2.47}$$

In the case where the relaxation associated with the emission of a photoelectron is small, $\Psi_f(N-1)$ is hardly different from $\Psi_g(N-1)$. Therefore we have

$$|<\Psi_f(N-1) \mid \Psi_g(N-1)>|^2 = 1. \tag{2.48}$$

From the definitions given in (1.4) and (1.11), we have

$$\boldsymbol{e}_B = -\boldsymbol{e}_i, \tag{2.49}$$

if the relaxation energy is almost zero. Thus, the photoelectron intensity distribution is given as

$$N(\boldsymbol{e}, \hbar\boldsymbol{w}) = A\sum_{m,i} \left|\langle m \mid p_e \mid i\rangle\right|^2 \boldsymbol{d}(\boldsymbol{e}_m - \boldsymbol{e}_B - \hbar\boldsymbol{w})\boldsymbol{d}(\boldsymbol{e} + \boldsymbol{e}_B). \tag{2.50}$$

Here we use the energy band model to describe one-electron states which are described as

$$\begin{cases} |m\rangle = |c, \mathbf{k}'\rangle \\ |i\rangle = |v, k\rangle \end{cases} \tag{2.51}$$

$$\begin{cases} \varepsilon_m = \varepsilon_{c\mathbf{k}'} \\ \varepsilon_B = -\varepsilon_{v\mathbf{k}} \end{cases}. \qquad (2.52)$$

Here we use $\mathbf{k}'$ and $\mathbf{k}$ only in the first Brillouin zero. In the case it is a well-known fact that transition matrix element is not zero only if the following condition is satisfied:

$$\mathbf{k}' = \mathbf{k} - \mathbf{G} \qquad (2.53)$$

Thus, (2.50) is written in the energy band picture described in the reduced zone scheme as

$$N(\varepsilon_B, \hbar\omega) = \sum_{c,\mathbf{K}',v,\mathbf{k},\mathbf{G}} |< c,\mathbf{k}'|p_e\,|\,v,\mathbf{k}>|^2\, \delta(\mathbf{k}'-\mathbf{k}-\mathbf{G}) \cdot \delta(\varepsilon_{c\mathbf{k}'} - \varepsilon_{v\mathbf{k}} - \hbar\omega) \cdot \delta(\varepsilon_{v\mathbf{k}} + \varepsilon_B). \qquad (2.54)$$

In practice, $\hbar\omega$ is large for the excitation in the soft x-ray region as compared with the binding energy $|\varepsilon_{v\mathbf{k}}|$. Then there are conduction states, c, satisfying the momentum conservation (2.53) for any v and $\mathbf{k}$. Therefore, we write $|\hbar\omega - \varepsilon_B, \mathbf{k}'>$ instead of $|c, \mathbf{k}'>$ and ignore the selection of special bands c. Thus, making summation over $\mathbf{k}'$ and c, we obtain

$$N(\varepsilon_B, \hbar\omega) = A \sum_{v,\mathbf{k},\mathbf{G}} |< \hbar\omega - \varepsilon_B, \mathbf{k} - \mathbf{G}\,|p_e\,|\,v,\mathbf{k}>|^2\, \delta(\varepsilon_{v\mathbf{k}} + \varepsilon_B). \qquad (2.55)$$

This formula describes the essence of the photoelectron spectroscopy of the energy band.

In angle integrated mode measurements, photoelectrons with all possible crystal momenta $\mathbf{k}$ are collected. This mode of measurement is realized by using a sample consisting of randomly oriented small grains like one deposited by the vacuum evaporation method. The transition matrix element can be replaced with its average over all possible $\mathbf{k}$ as

$$\sum_{\nu,\mathbf{k},\mathbf{G}} |< \hbar\omega - \varepsilon_B, \mathbf{k} - \mathbf{G} | p_e | \nu, \mathbf{k} >|^2 = | M_l(\hbar\omega) |^2 . \qquad (2.56)$$

Here it is taken into account that the transition matrix element is very much dependent on the orbital symmetry, the azimuthal quantum number l. The valence band density of states is given as

$$D(\varepsilon_B) = \sum_{\nu\mathbf{k}} D_l(\varepsilon_B) \qquad (2.57)$$

Thus, we approximate the intensity distribution given by (2.55) as

$$N(\varepsilon_B, \hbar\omega) = A \sum | M_l(\hbar\omega) |^2 D_l(\varepsilon_B) . \qquad (2.58)$$

The relaxation energy is not always small and (2.48) is not always satisfied. So, under this condition, the one-electron approximation does not hold and we have to make the many- electron approximation. It should be pointed out that the relaxation effects are brought about the many-electron interaction based on the exchange and Coulomb interactions. The typical example is the occurrence of the satellite lines. Another example of the break down of the simple one-electron picture described by (2.50) is the thing that the Auger interaction V_A cannot be ignored. In this case, the resonant photoemission occurs.

Not only the intrinsic many-electron interactions pertuning to the optical excitations but also another source causes additional lines in a photoemission spectrum. A photoexcited electron travels a relatively long way from the place, at which the electron is excited to the surface. It is possible to excite other electrons existing in the solid. Such a satellite has a definite structure when the primary photoelectron excites plasmons. These extract satellites are called the plasmon satellites.

2.4 Energy Analysis of Photoelectron

A very important measurement in photoemission experiment is the energy analysis of photoelectron. A photoemission experiment is carried out as follow:

(i) A sample is exposed to monochromatic excitation light with an energy $\hbar\omega$.

(ii) Photoelectrons are emitted from the sample.

(iii) The kinetic energies of photoelectrons are analyzed. Photoelectrons with a kinetic energy of ε_k are selected and its intensity defined as the number of photoelectron, $N(\varepsilon_k)$, emitted forward a special direction set up by structural instrumental arrangement is measured.

(iv) The instrument to select photoelectrons according to their kinetic energies is called the energy analyzer.

(v) The kinetic energy to be measured is changed and the intensity of the photoelectrons is measured. The curve showing $N(\varepsilon_k)$ versus ε_k is called the energy distribution curve. The energy distribution curve is also called the photoemission spectrum.

(vi) The intensity of photoelectrons is also dependent on the excitation energy. Thus, the energy distribution curve is written as

$$N(\varepsilon_k, \hbar\omega) \text{ versus } \varepsilon_k$$

(vii) If ε_k is fixed and the photon energy is varied, the resulting spectrum

$$N(\varepsilon_k, \hbar\omega) \text{ versus } \varepsilon_k$$

is called the partial photoyield spectrum.

(viii) If all photoelectrons with different kinetic energies are collected as

$$N(\hbar\omega) = \int N(\varepsilon_k, \hbar\omega) d\varepsilon_k \ , \qquad (2.59)$$

resulting spectrum

$$N(\varepsilon_k, \hbar\omega) \text{ versus } \varepsilon_k$$

is called the total photoyield spectrum.

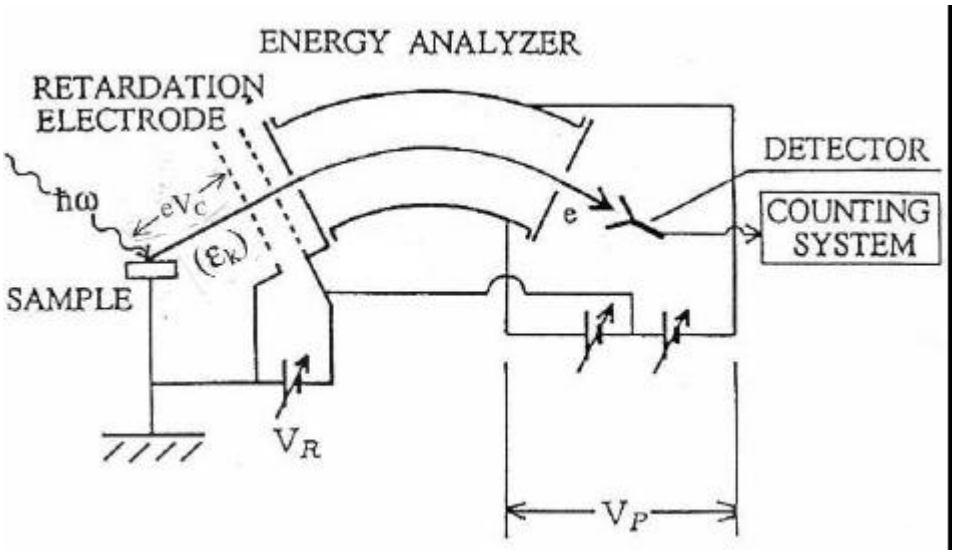

Figure 2.5. Experimental arrangement for measuring the kinetic energies of photoelectrons.
e_k : Kinetic energy in a free space.
V_R : Retardation voltage.
V_P : Voltage applied to energy analyzer electrodes.

In fig 2.5, the principle of the photoelectron energy analysis is shown. First, suppose the sample is electrically grounded. If photoelectrons leave the sample with a kinetic energy e_k, the energy is equivalent to a potential energy corresponding to

$$e_k = bV_e \ . \qquad (2.60)$$

In practice, we use an energy analyzer of the electrostatic type. It consists of a pair of electrodes to form an electrostatic field with a potential V_P. A more detailed description of the energy analyzer will be made later.

We use an electrode giving a retardation field V_R in front of the entrance slit of the energy analyzer. Then, photoelectron loses the energy equal to eV_R before it arrives the entrance slit of the energy analyzer. The energy analyzer is designed that photoelectron with an energy equals to aV_P can pass through it. a is a constant determined by the structure and the size of the energy analyzer. Thus, we have the

contact potential V_C exists between the sample surface and the analyzer system. This contact potential retard photoelectrons by and energy equal to eV_C. Thus, we have

$$\varepsilon_k - eV_C - eV_R = \alpha V_P . \qquad (2.61)$$

However the sum of the work function of the sample and the contact potential between the sample surface and the analyzer system is equal to the work function of the analyzer system $e\phi_s$ which is practically that of the material forming the retardation electrode. Thus, we have

$$\varepsilon_k - (e\phi_s - e\phi) = eV_R + \alpha V_P \qquad (2.62)$$

Using (1.5) we get

$$\hbar\omega - \varepsilon_B - e\phi - (e\phi_s - e\phi) = eV_R + \alpha V_P \qquad (2.63)$$

then we have

$$\varepsilon_B = \hbar\omega - e\phi_s - eV_R - \alpha V_P \qquad (2.64)$$

It should be remarked that the binding energy of photoelectrons can be measured by scanning either V_R or V_P and it is independent on the work function of the sample. Since constants α and $e\phi_s$ can be obtained separately, we can obtain ε_B from (2.64).

Four different types of energy analyzer are shown schematically in Fig 2.6. In the figure, panel (a) shows the parallel plate energy analyzer. The electric field pulls the electrons toward the positive electrode direction and they make parabolic trajectories in the analyzer field. If the potential formed by the electrodes is fixed and the distance between the entrance and exit slits is fixed then the energy of electrons that can pass the analyzer field is decided. This is the principle of the energy analysis. Other types of the analyzer, (b) the hemispherical type, (c) the cylindrical type and (d)

the cylindrical mirror type, select the electron energy by the similar principles. The characteristics of these types energy analyzer are shown in Table 2.1

Table 2.1

Some important characteristics of electrostatic electron energy analyzer. Only the 1st order values of the energy resolving power are indicated.

	Type / Characteristics	Parallel Plate	Spherical	Cylindrical
1	Focus condition	Incident angle 45^o	Deviation angle 180^o	Deviation angle 127^o
2	Energy for the central orbit	$\boldsymbol{e}_0 = eV_P \dfrac{L_0}{2S}$	$\boldsymbol{e}_0 = eV_P \Big/ (\dfrac{R_2}{R_1} - \dfrac{R_1}{R_2})$	$\boldsymbol{e}_0 = eV_P \Big/ 2\ln(\dfrac{R_2}{R_1})$
3	Resolving power	$\dfrac{\Delta \boldsymbol{e}_k}{\boldsymbol{e}_0} = \dfrac{2\boldsymbol{w}}{L_0}$	$\dfrac{\Delta \boldsymbol{e}_k}{\boldsymbol{e}_0} = \dfrac{2\boldsymbol{w}}{R_0}$	$\dfrac{\Delta \boldsymbol{e}_k}{\boldsymbol{e}_0} = \dfrac{2\boldsymbol{w}}{R_0}$

L_0 : Distance between the entrance and exit slit.

R_0 : Radius of the central orbit.

$\boldsymbol{e}_0$: Energy corresponding to the central orbit.

R_1 : Radius of the inner electrode.

R_2 : Radius of the outer electrode.

V_P : Potential difference between two electrodes.

$\boldsymbol{w}$: Slit width.

The values of energy resolving power in the 1st order approximation are presented there. In the higher order approximation the resolving power is dependent on the square of the angular divergence of the electrons incident on the analyzer. The energy corresponding to the central trajectory is proportional to the potential applied to the analyzer electrodes. The proportionality constant is determined by the analyzer geometry. Another distinctive aspect is that the resolving power is constant, which is also decided by geometrical parameters.

Detectors of photoelectrons are electron multipliers. In an electron multiplier, an electron hits the electron target and generates secondary electrons. A secondary electron produced is accelerated between adjacent electrodes and hits the neighboring electrode, where it produces more than two secondary electrons. By successive repetition of this secondary electron generation, the number of electrons generated comes up to he values of 10^6, and they are detected as a pulse current. If the electrode

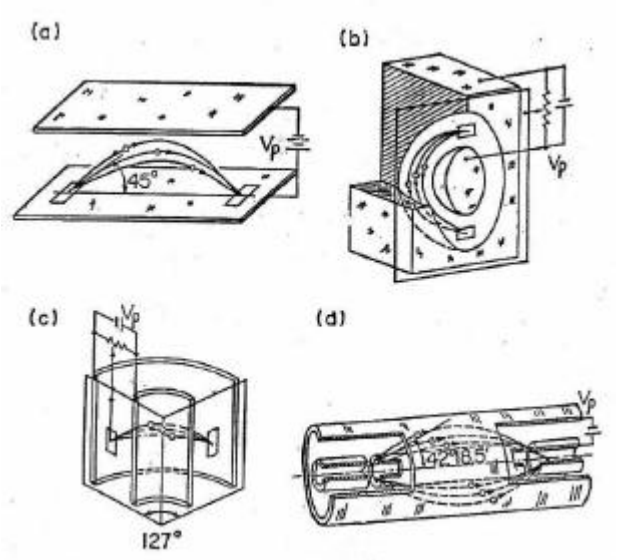

Figure 2.6. Principle of operation of electron energy analyzer.
(a) Parallel plate energy analyzer.
(b) Hemispherical energy analyzer.
(c) Cylindrical energy analyzer.
(d) Cylindrical mirror energy analyzer.

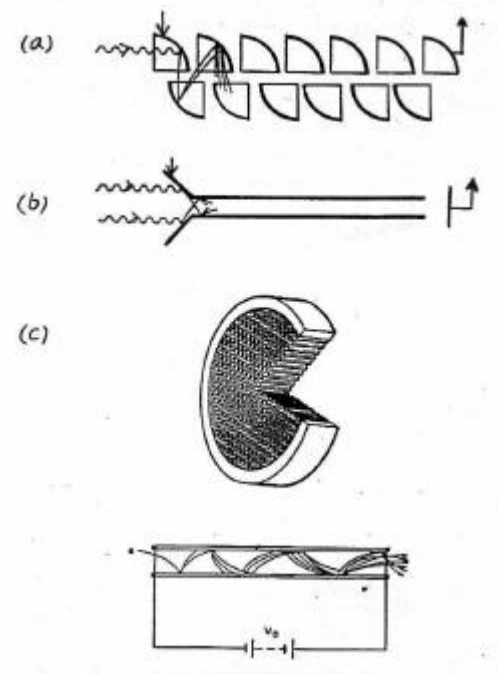

Figure 2.7. Principle of operation of electron multipliers.
(a) Photoelectron multiplier tube.
(b) Channeling electron multiplier.
(c) Multi channel electron multiplier.

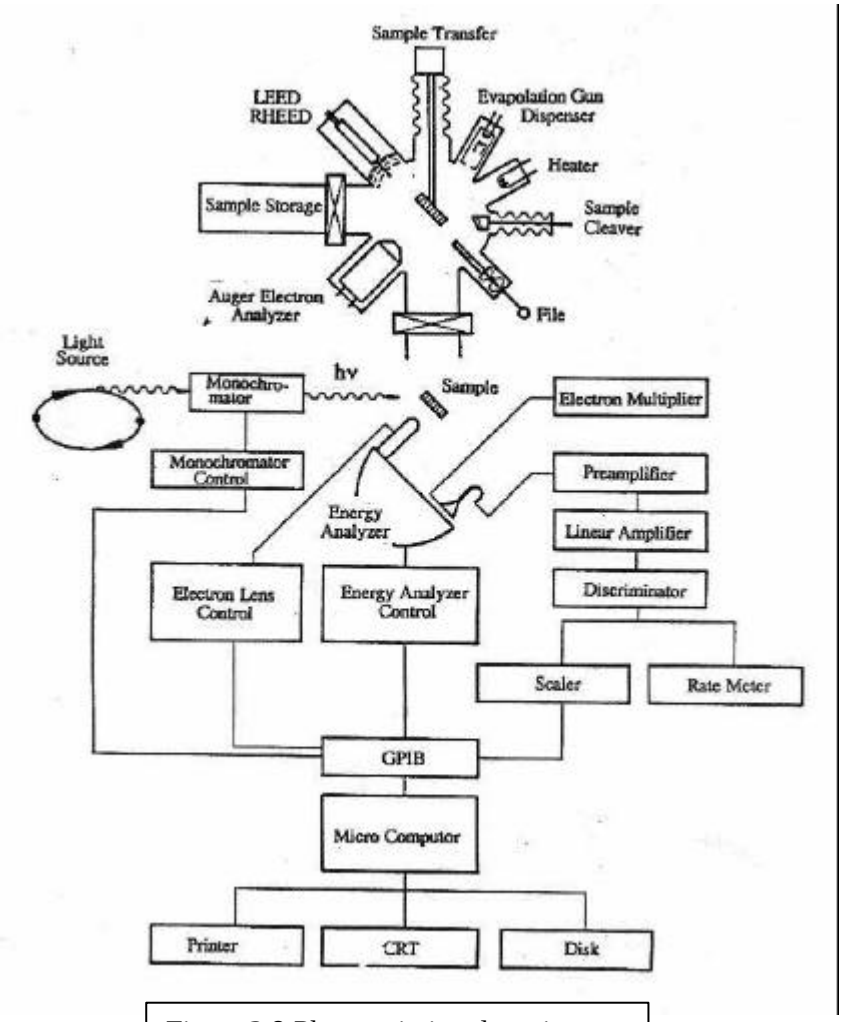

Figure 2.8 Photoemission detection.

is designed just as a tube where the potential gradient is imposed by flowing small current across a high resistivity.

The device like this is called channeling electron multiplier. The principle of the electron multiplier is shown is in Fig 2.7. If very thin channeling electron multipliers are board together, it can be used for two dimensional detection. The device is also shown in Fig 2.7.

The current pulses are counted and taken as the photoelectron numbers. The electronic system for the photoelectron detection is shown in schematically Fig 2.8. No further explanation of the circuit is made here.

2.5 Photoemission Spectroscopy of Metallic Nickel

We will see the experimental results of the photoemission spectra of metallic nickel. From periodic table, we know that the electronic configuration of Ni atom is $1s^2 2s^2 2p^6 3s^2 3p^6 3d^8 4s^2$ with 5 spin-up and 3 spin-down electrons in the 3d orbit. The XPS spectra of the 3d, 3p, 3s, $2p_{1/2}$ and $2p_{3/2}$ levels of Ni metal are shown from Fig.2.9. They are the spectra of the valence band and the core level with binding energies lower than 1000ev. The values of the binding energy are shown below each spectrum. The XPS spectra cannot be measured with an energy resolution better than about 0.8eV. This is because the intensity of x-rays used for exciting photoelectrons, either $AlK\alpha_{1,2}$ (1.468keV) or $MgK\alpha_{1,2}$ line (1.257keV), is not strong enough for them to be monochromatized to a narrow line. Even if the monochromatization with a resolving power of 5000eV is realized, the resulting resolution is about 0.25eV.

In the core level lines, the multiple structures are expected to be observed. In the case of the 3p spectrum, the coupling between the 3d electrons and 3p holes through the exchange interaction can give rise the multiple splitting observable with as low resolution as 1.0eV. In the 3p spectrum shown in Fig.2.9, such structures are not found. It may be ascribed by the fact that 3p electrons in metallic nickel are itinerant to a considerable extent and not much localized so that the exchange integral between the 3p and 3d states is not large enough to cause the observable multiple splitting, the main line peak around 66eV has the composite structure. It is caused by the spin-orbit splitting of the 3p-hole level; the $3p_{3/2}$ is expected to occur at 66.2eV and $3p_{1/2}$ at 68.0eV.

Figure 2.9 shows the existence of a satellite line around 6eV below the main line. In the valence shell spectra, a feature is found 6eV below the main band. Wertheim and *Hüfner* showed that similar features also occur in the spectra of core level lines in Fig 2.9. There were a lot of arguments concerning the origin of the feature. In the figure, features aligned on the vertical line designated as satellite are the features under question. Since the features are common among various core level lines, their origins were considered to be practically the same.

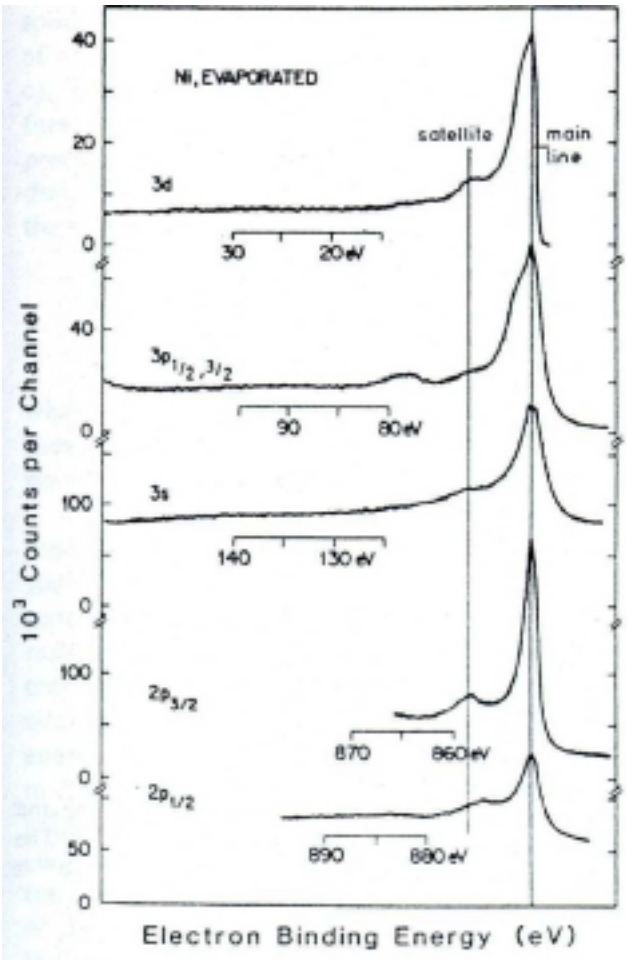

Figure 2.9. XPS spectra of the 3d, 3p, 3s, $2p_{3/2}$, and $2p_{1/2}$ levels of Ni metal. The main lines have been lined up to demonstrate the constant distant of the satellite position. (*Hüfner* , S. 1975)

The feature is now called the 6eV satellite or the two-hole bound state satellite. Some explanations were represented in the past. One of the explanations is impurity. But the high quality sample preparation and chemical analysis of the surface expels it. Another explanation is band structure effects. But the data of angle—resolved photoemission spectroscopy disagree with this idea. Also people regarded the idea that the structure is the plasmon sideband. It is the most possible reason owing to the character of a metal. It is further plausible, because the feature is common among all the core level lines. However, the loss function, as measured by optical means or by electron energy loss experiments does not show any structure at energy around 6eV. Therefore, the only possible explanation in terms of final state effects is left.

Figure 2.10 gives a schematic band structure of nickel metal in the initial state, where the $3d^9$ state, the 3d band, lies within the 4s-band. Both of the 3d and 4s band are partially filled and the parts of the bands are located above or under Fermi level.

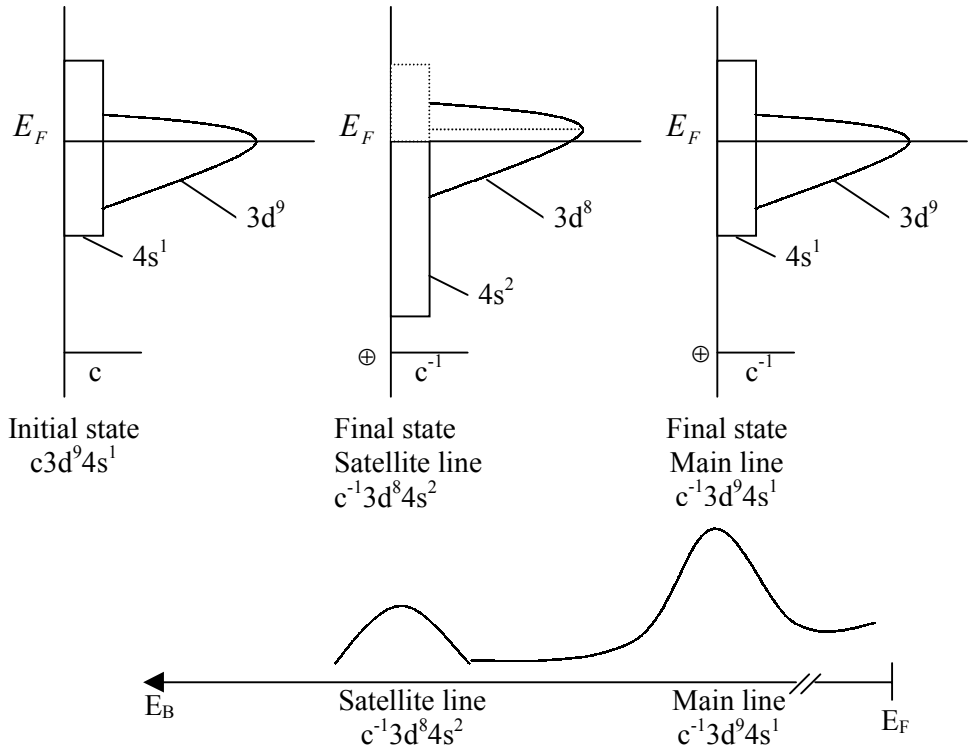

Figure2.10. Schematic density of states of Ni, indicating the origin of the main line and the satellite for core ionization (c^{-1}); The initial state is $c3d^84s^2$ and the two final state are $c^{-1}3d^94s^1$ (satellite) and $c^{-1}3d^{10}4s$ (main line); c denotes a core level, c^{-1} a core hole.

In the final state of the photoemission from a core level, a hole exists in the core level and this alters the valence state considerably, because the core hole potential changes the valence state in a way that extra electron-electron interaction is generated in a comparatively localized state. In the sense of equations (2.44) and (2.45), the many electron state, $\left|\Psi_f(N-1)\right\rangle$, is different from $\left|\Psi_g(N-1)\right\rangle$. By solving many-electron hamiltomian, one can prove that there are two many electron final states with eigen energies E_1 and E_2 where

$$E_2 = E_1 + 6eV\,. \qquad (2.65)$$

The transition to the E_2 state generates the feature at a binding energy higher than E_1 band by 6eV. The occurrence of the two final states is explained by the states, but it is qualitatively understandable as follows: In the atomic level notation, the ground state configuration of the nickel atom in the metallic state is $3d^94s$. This means that the

energy band of nickel is filled up to the state in which average change density of nickel is such that 9 electrons in the 3d orbitals and 1 electron in the 4s orbital. Since the 3d band is filled up with 10 electrons per atom, the $3d^9$ state is equivalent to the one-hole state in the 3d band. As far as the electronic configuration is concerned, the $3d^84s^2$ state is also possible. According to the existing solid state data such as the magnetization, the Mossbauer effect, the neutron diffraction and the specific heat, show that the number of average 3d electrons per atom is slightly larger than 9, the $3d^94s$ configuration is dominant in the ground state. This means that the state generated by the $3d^94s^1$ configuration has the energy higher than $3d^84s^2$ ground state.

Thus we assume the ground state $\left|\Psi_g(N-1)\right\rangle$, in which a core electron is missing, to be

$$\left|\Psi_g(N-1)\right\rangle = \left|3d^9 4s\right\rangle \equiv \varphi_1 \tag{2.66}$$

In the final state, the perturbation due to the existence of the core hole occurs. Because of the correlation potential caused by a core hole, the state originate in the $3d^84s^2$ configuration mixes into the $(N-1)$ state. Thus,

$$\left|\Psi_f(N-1)\right\rangle \equiv a\left|\varphi_1\right\rangle + b\left|\varphi_2\right\rangle \tag{2.67}$$

$$\left|\varphi_2\right\rangle \equiv \left|3d^8 4s^2\right\rangle \tag{2.68}$$

Let the hamiltonian in the ground state be H_0 and the corresponding eigen energy be E_0. Then we have

$$\begin{cases} H_0\left|\varphi_1\right\rangle = E_1\left|\varphi_1\right\rangle \\ H_0\left|\varphi_2\right\rangle = E_2\left|\varphi_2\right\rangle \end{cases} \tag{2.69}$$

In the final state, the hamiltonian is changed to

$$H = H_0 + \Delta H \tag{2.70}$$

where ΔH is the correlation energy caused by the core hole. The hamiltonian equation is

$$H\left|\Psi_f(N-1)\right\rangle = E\left|\Psi_f(N-1)\right\rangle \tag{2.71}$$

Therefore,

$$(H_0 + \Delta H)(a\left|\varphi_1\right\rangle + b\left|\varphi_2\right\rangle) = E(a\left|\varphi_1\right\rangle + b\left|\varphi_2\right\rangle) \tag{2.72}$$

Then the secular equation to solve (2.72) is

$$\begin{vmatrix} E_1 + \Delta H_{11} - E & \Delta H_{12} \\ \Delta H_{21} & E_2 + \Delta H_{22} - E \end{vmatrix} = 0 \tag{2.73}$$

$$\begin{cases} \left\langle \varphi_1 \left| \Delta H \right| \varphi_1 \right\rangle \equiv \Delta H_{11} \\ \left\langle \varphi_2 \left| \Delta H \right| \varphi_2 \right\rangle \equiv \Delta H_{22} \\ \left\langle \varphi_1 \left| \Delta H \right| \varphi_2 \right\rangle \equiv \Delta H_{12} \equiv \left\langle \varphi_2 \left| \Delta H \right| \varphi_1 \right\rangle \equiv \Delta H_{21} \equiv \Delta \end{cases} \tag{2.74}$$

If we put

$$\begin{cases} E_1 + \Delta H_{11} \equiv \hat{E}_1 \\ E_2 + \Delta H_{22} \equiv \hat{E}_2 \\ \hat{E}_2 - \hat{E}_1 \equiv \delta \end{cases} \tag{2.75}$$

The secular equation (2.73) is written as

$$\begin{vmatrix} \hat{E}_1 - E & \Delta \\ \Delta & \hat{E}_2 - E \end{vmatrix} = 0 \tag{2.76}$$

The solutions are

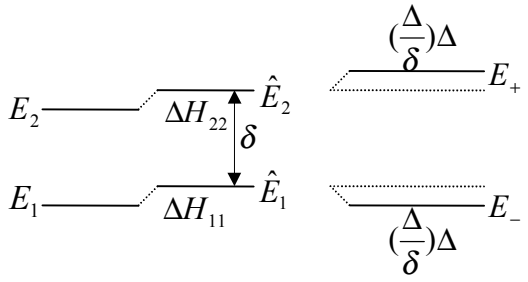

Figure 2.11 Energy diagram for the solutions of *Shrödinger* equation

$$\begin{cases} E = \hat{E}_2 + (\frac{\Delta}{\delta})\Delta \equiv E_+ \\ or\ \hat{E}_1 - (\frac{\Delta}{\delta})\Delta \equiv E_- \end{cases} \tag{2.77}$$

Here the assumption is made that

$$\begin{cases} \hat{E}_2 > \hat{E}_1 \\ \delta >> \Delta \end{cases}$$

The final state eigen functions are

$$\begin{cases} \Psi_f^+(N-1) = (\frac{\Delta}{\delta})\left|\varphi_1\right\rangle + \sqrt{1-(\frac{\Delta}{\delta})^2}\left|\varphi_2\right\rangle \\ for \quad E = E_+ = E_2 + \Delta H_{22} + (\frac{\Delta H_{11}}{E_2 - E_1 + \Delta H_{22} - \Delta H_{11}})^2 \Delta H_{12} \end{cases} \tag{2.78}$$

$$\begin{cases} \Psi_f^-(N-1) = \sqrt{1-(\frac{\Delta}{\delta})^2}\left|\varphi_1\right\rangle - (\frac{\Delta}{\delta})\left|\varphi_2\right\rangle \\ for \quad E = E_- = E_1 + \Delta H_{11} - (\frac{\Delta H_{11}}{E_2 - E_1 + \Delta H_{22} - \Delta H_{11}})^2 \Delta H_{12} \end{cases} \tag{2.79}$$

If the state is $\left|3d^9 4s\right\rangle$ in the ground state with energy E_1, the spectral weight for the transition to E_+ state is given as

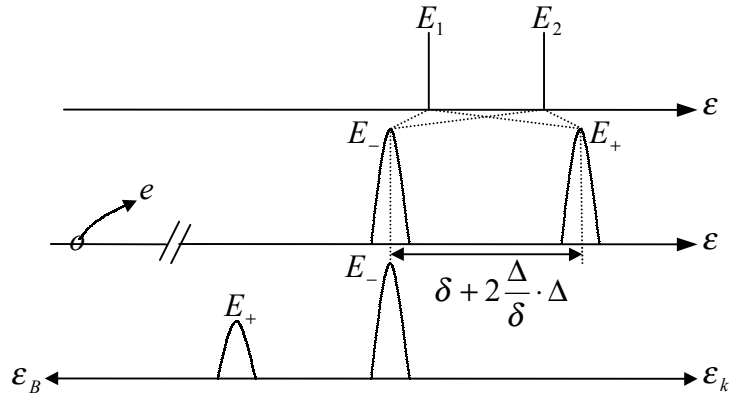

Figure 2.12 Diagram for the transition from initial states to the two calculated energy states.

$$\begin{aligned}\left|\left\langle \Psi_f^+(N-1)\middle\| \Psi_g(N-1)\right\rangle\right|^2 &= \left|\left\langle \Psi_f^+(N-1)\middle| 3d^9 4s\right\rangle\right|^2 \\ &= (\frac{\Delta}{\delta})^2\end{aligned} \tag{2.80}$$

Similarly, the spectral weight for the transition to E_- is given as

$$\begin{aligned}\left|\left\langle \Psi_f^-(N-1)\middle\| \Psi_g(N-1)\right\rangle\right|^2 &= \left|\left\langle \Psi_f^-(N-1)\middle| 3d^9 4s\right\rangle\right|^2 \\ &= 1-(\frac{\Delta}{\delta})^2\end{aligned} \tag{2.81}$$

In the explanation described above, the core hole generated play a role to provide the perturbation for exciting the E^+ state. Its effect manifests itself as ΔH and thus as Δ above. We will come back to this point later.

In the case of the valence shell excitation, the situation appears to be more complicated, since the hole is incorporated by a photon in the valence shell. Then the two base states describing the final state could be

$$\begin{cases} \left|\varphi_1\right\rangle \equiv \left|3d^9\right\rangle \\ \left|\varphi_2\right\rangle \equiv \left|3d^8 4s\right\rangle \end{cases} \tag{2.82}$$

instead of $\left|3d^9 4s\right\rangle$ and $\left|3d^8 4s^2\right\rangle$ in innershell excitation. The all other mathematical treatments are the similar to those described above and the results are the same as those given by equations (2.78) and (2.79). The spectral weight is not so simple as those equations (2.80) and (2.81). In order to show the concept only, we ignore rigorousness and assume that the ground state eigenfunction is given as

$$\begin{aligned}\left|\Psi_g\right\rangle &= \alpha\left|4s\right\rangle\left|\varphi_1\right\rangle + \beta\left|3d\right\rangle\left|\varphi_2\right\rangle \\ &= \alpha\left|4s\right\rangle\left|3d^9\right\rangle + \beta\left|3d\right\rangle\left|3d^8 4s\right\rangle\end{aligned} \tag{2.83}$$

and the final state eigenfunctions are given as

$$\begin{cases}\left|\Psi_f^+\right\rangle = \left|\varepsilon_k\right\rangle\left|\Psi_f^+(N-1)\right\rangle & for\ E^+\ state \\ \left|\Psi_f^-\right\rangle = \left|\varepsilon_k\right\rangle\left|\Psi_f^-(N-1)\right\rangle & for\ E^-\ stat\end{cases}, \tag{2.84}$$

the transition matrix elements are given as

$$\left|\left\langle\Psi_f^+\left|T\right|\Psi_g\right\rangle\right|^2 = \left|\alpha\right|^2 \cdot \left|\left\langle\varepsilon_k\left|\mathbf{p}\right|4s\right\rangle\right|^2 (\frac{\Delta}{\delta})^2 + \left|\beta\right|^2 \cdot \left|\left\langle\varepsilon_k\left|\mathbf{p}\right|3d\right\rangle\right|^2 (1-(\frac{\Delta}{\delta})^2) \tag{2.85}$$

$$for\ the\ transition\ g \to E^+$$

$$\left|\left\langle\Psi_f^-\left|T\right|\Psi_g\right\rangle\right|^2 = \left|\alpha\right|^2 \cdot \left|\left\langle\varepsilon_k\left|\mathbf{p}\right|4s\right\rangle\right|^2 (1-(\frac{\Delta}{\delta})^2)(\frac{\Delta}{\delta})^2 + \left|\beta\right|^2 \cdot \left|\left\langle\varepsilon_k\left|\mathbf{p}\right|3d\right\rangle\right|^2 (\frac{\Delta}{\delta})^2 \tag{2.86}$$

$$for\ the\ transition\ g \to E^-$$

Here we ignored the cross terms

$$\alpha^*\beta\left\langle\varepsilon_k\left|\mathbf{p}\right|4s\right\rangle^*\left\langle\varepsilon_k\left|\mathbf{p}\right|3d\right\rangle(\frac{\Delta}{\delta})\sqrt{1-(\frac{\Delta}{\delta})^2} + c.c.$$

In many cases, the cross terms are small. If the cross terms are not negligible, the interference effect follows. Since the ground state can be described by the energy band picture, decomposition as shown in (2.83) comprises many terms. In the case of the atomic spectra and the crystal field spectra, where the multiple coupling and/or the

crystalline field effect dominated, coefficients α and β include the factors like the Clebsch-Gordan coefficients, 6j-symbols and the coefficients of fractional parentage appear

$$\begin{array}{l} \textit{ground state} \quad \textit{final state} \\ (3d^9 4s) \xrightarrow{\eta\omega} (3d^9 4s)^{-1} + e \rightarrow (3d^9) + e \\ \qquad\qquad\qquad\qquad\qquad\qquad \rightarrow (3d^8 4s) + e \\ (3\hat{d}\,4s) \xrightarrow{\eta\omega} (3\hat{d}\,4\hat{s}) + e \\ \qquad\qquad\qquad\quad (3\hat{d}\,3\hat{d}\,4s) + e \\ \qquad\qquad\qquad\quad (3\hat{d}^{\,2}\,4s) + e \end{array}$$

For the valence shell state, we postulated so far that there are two basic final state configurations, $3d^9$ and $3d^8 4s$. However, this has to be considered more carefully. First the configuration is for one Ni atom. So we have not taken the solid state effect at this stage. Second the satellite splitting is governed by the quantity designated as δ. We have not taken insight in this quantity. Third, the theoretical foundation of the two different final states is not given.

In the present argument, the ground state, $3d^9 4s$, represents the many-electron state generated by energy band electrons. Thus the corresponding eigen energy has just a single value given by the sum of all the electrons occupying the band. The situations for the two final states, $3d^9$ and $3d^8 4s$, are more or less similar. However the eigen energy for them is not a single value. The value spreads since there are many $3d^9$ and $3d^8 4s$ states with different $4s^{-1}$ states, the hole states in the conduction bands.

This aspect is better understandable if we consider the hole states. The ground state is described as the one 3d-hole state $3\hat{d}$, since the 4s band is only half filled and do not consider the unfilled part as the hole state. If an incident photon ejects a 4s electron form the sample, a 4s hole, $4\hat{s}$, is added to the sample. If a photon ejects a 3d electron, a 3d hole is added. Obviously, there are two distinctly different cases. The added hole can migrate in the crystal jumping from site to site, since it occupies the energy bands. The state like this is represented as ($3\hat{d}3\hat{d}4s$). In this state, 3d holes are moving independently of each other.

Suppose two 3d holes exist on the same lattice site. The holes repels each other by the electrostatic repulsion. Particularly, the exchange interaction increases the state energy by an amount denoted so far as δ or $\hat{\delta}$. If such two holes exist at one lattice site, conduction electrons approach the site to screen the extra change incorporated by two holes. In the balance of the exchange repulsion and the screening by conduction electrons, the two holes can be kept located at the same lattice site forming a stable state. This state is called the two-hole bound states and represented as $3\hat{d}^2 4s$ here.

The most important issue in the argument of the 6eV satellite is to prove that the two-hole bound state does exist. This has been carried out many authors. Their arguments are based on the Hubband model. Thus they started with the view that 3d electrons are itinerant. The exchange interactions in the system with one hole per atom at the beginning generate poles in the spectrum function, the green function, that leads the peaks in the spectrum function. One of them gives a peak about several electron volts below the main peak. The treatments like this show not only the existence of the satellite but also the existence of a stable two-hole state or a single site. They also show that the electronic structure of metallic nickel in the final state of photoemission cannot be well explained in terms of the energy band picture only.

The 6eV satellite in the core level line can be explained similarly. However there is an essential difference in one issue. The aspect which is similar to the case of the valence shell spectrum is that the occurrence of the satellite is the reflection of the energy state of the valence electrons. The aspect that is quite different is that both the satellite and main line are the line spectra. This shows that the valence shell energy state should be treated as an atomic states. The strong correlation interaction caused by the core hole changes the valence shell state in a way the itinerant nature is lost and the state under problem is localized on the atom where the core hole is located. If the atomically localized nickel electrons seeing the core hole potential take the configuration $3d^8 4s^2$, the important interaction between 3d electrons is the exchange interaction. This explain the two-hole bound state satellite occurs at the same energy apart from the main line. In this 6eV satellite state, the energy band picture collaps

completely. This type of the many-electron interaction is brought about by the photoproduced hole.

In the argument of the 6eV satellite of nickel, some seemingly different qualitative interpretations are proposed. They explain a property of photoexcitation. As we have seen already, the satellite is a result of the interaction between localized electrons in an atom of metal and this interaction occurs only in the final state in the photoemission process. Thus, the spectral feature like this is mentioned to be caused by "the final state interaction" or, using a term from the atomic spectrum not quite appropriately, "the post collision interaction." As mentioned already, this is a typical example of "the collapse of the energy band picture."

We have seen that the core level satellite is caused by the core hole potential suddenly generated by photoexcitation. It changes the outershell electronic structure so that they are more localized on the core hole site and the correlation interaction is enhanced. Just for the convenience for the explanation, we suppose the final state interaction is that a 3d electron is excited to the unoccupied 4s level. In analogy to a similar excitation in the case of the photoemission spectra of some rare gases, we call this the shake up transition. We take the process as if an electron is being lifted up during the course of the shaking of the orbit by the incident electromagnetic oscillatory field of a photon. In this sense, the satellite is called the shake up satellite.

Since the 6eV satellite appears as if a level exist 6eV below the level leading to the main line and this lowering of the level is caused by the photoproduced core hole. Therefore, the satellite is often called the shake down satellite. As mentioned already, movile and immovile 3d holes are generated by photoexcitation: $3\hat{d}3\hat{d}$ and $3\hat{d}^2$. In case of immovile holes, the two bound holes, they attract more conduction electrons to screen the pair. In this sense, the satellite is called the well-screened peak by some authors. On the other hand, the main line is called the poorly screened peak. The shake-up, the shake-down and the well screened peaks are just the name given without a well established quantum mechanical treatment. The two-hole bound state and the theoretical calculation based on the many-electron quantum mechanics are the correct one. The idea of the two-hole bound state was first proposed by N. F. Mott long time ago. He referred to the energy band calculation by J. Kanamori as the basis of the concept.

In practice, the hamiltonian of the system is given as

$$H = \sum_{\mathbf{k}\sigma} \varepsilon_{\mathbf{k}\sigma} d^{+}_{\mathbf{k}\sigma} d_{\mathbf{k}\sigma} + U \sum_{i} d^{+}_{\uparrow i} d_{\uparrow i} d^{+}_{\downarrow i} d_{\downarrow i} \ . \qquad (2.87)$$

Here $\varepsilon_{\mathbf{k}\sigma}$ is the energy of a conduction electron, $d^{+}_{k\sigma}$ and $d_{\mathbf{k}\sigma}$ are the creation and annihilation operators of the conduction electron. Here we consider d electrons are also itinerant. d^{+}_{σ} is the creation and annihilation operators of the electrons bound on the nickel atom where the photoproduced hole is located. The hamiltonian can be solved the most simply by adopting the random phase approximation. U is the exchange energy between d electrons bound on the extra hoe site. This equation is solved under the assumption that two holes exist in one site. Different authors have used different types of the Feynmann diagrams, but for the final result they have obtained are not much different. The spectrum function leads to the density of state (Green's function) is given as

$$\begin{cases} G(\mathbf{k}\sigma,\varepsilon) = \dfrac{f_{\mathbf{k}\sigma}}{\varepsilon - \varepsilon_{\mathbf{k}\sigma} - S(\mathbf{k}\sigma,\varepsilon) + i0^{+}} \\ S(\mathbf{k}\sigma,\varepsilon) = -\sum\limits_{\mathbf{k'}} (1 - f_{\mathbf{k'}\sigma}) \dfrac{U}{1 + U G^{0}_{\mathbf{k}\sigma,\mathbf{k'}\sigma}(\varepsilon + \varepsilon_{\mathbf{k'}\sigma})} \\ G^{0}_{\mathbf{k}\sigma,\mathbf{k'}\sigma} = \sum\limits_{\mathbf{q}} \dfrac{f_{\mathbf{k}+\mathbf{q}} \ f_{\mathbf{k'}-\mathbf{q}}}{\varepsilon - \varepsilon_{\mathbf{k}+\mathbf{q}} - \varepsilon_{\mathbf{k'}-\mathbf{q}} - i0^{+}} \end{cases} \qquad (2.88)$$

Here $f_{\mathbf{k}\sigma}$ is the Fermi-Drack distrbution function. The density of states is given as

$$D(\varepsilon) = \frac{1}{\pi} \mathrm{Im} \sum_{\mathbf{k}\sigma} G(\mathbf{k}\sigma,\varepsilon) \qquad (2.89)$$

the pole in the Green function is obtained by solving

$$\varepsilon - \varepsilon_{\mathbf{k}\sigma} - S(\mathbf{k}\sigma,\varepsilon) = 0 \qquad (2.90)$$

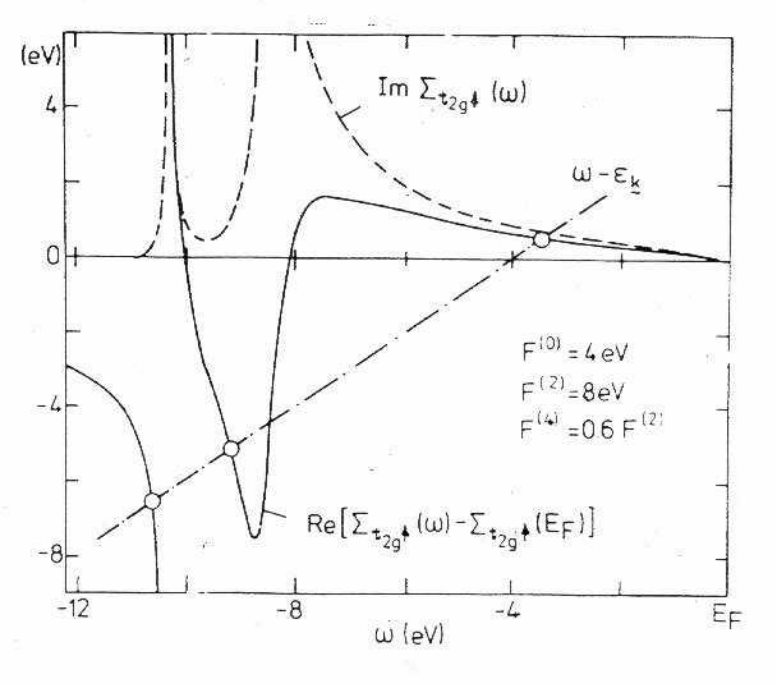

Figure 2.13 The result of numerical calculation.

thus the poles are given as the cross points between two curves

$$\begin{cases}\omega = S(\mathbf{k}\sigma,\varepsilon) \\ \omega = \varepsilon - \varepsilon_{\mathbf{k}\sigma}\end{cases}. \tag{2.91}$$

Fig 13 shows the result of numerical calculation of the curve $\omega = S(\mathbf{k}\sigma,\varepsilon)$ and with that of $\omega = \varepsilon - \varepsilon_{\mathbf{k}\sigma}$. Circles in the curve show the cross points. This one point present the location of the main band (center gravity!) and other two the satellites. Third line corresponding to the pole has recently been found, although the peak intensity is very weak. In this way multihole bound state satellite has been theoretically established.

In order to show the more convincing evidence to support the two-hole assignment for the 6-ev satellite in valence band of Ni metal, we have to mention resonance photoemission briefly here. The use of energy tunability of synchrotron radiation is crucial for performing the resonant photoemission, which is a phenomenon that the ionization cross sections of outershell electrons are enhanced

enormously for excitations above the threshold of an innershelle excitation. The fundamentals of the resonance mechanism was worked out by Fano for suggesting the line shape of the autoionization spectrum. The main part of the valence band photoemission in the transition metal is brought about by the photoionization of the 3d electron. In the atomic notations, the transition is written as

$$3p^6 3d^N \xrightarrow{\eta\omega} 3p^6 3d^{N-1}\varepsilon l . \tag{2.92}$$

The final state, $3p^6 3d^{N-1}\varepsilon l$, can be reached by the transition as

$$3p^6 3d^N \xrightarrow{\eta\omega} 3p^5 3d^{N+1} \xrightarrow{Auger} 3p^6 3d^{N-1}\varepsilon l \tag{2.93}$$

If the two processes, the photoabsorpton of the 3p electron and the subsequent Auger transition, occur instantanously, the transition looks like one given as (2.92) as whole, and the situation is the resonance between the innershell excitation $3p \to 3d$ and the outshell excitation $3d \to \varepsilon l$. As a result, the ionization cross section of the 3d electron is enhanced above the threshold for the $3p \to 3d$ excitation. In this case, what gives rise to the resonance is the second term of the T-matrix operator given as (1.18).

In the process expressed as (2.93), the state, $3p^5 3d^{N+1}$, is an intermediate state. Let us refer to the basis function of such an intermediate state as $|\Psi_u\rangle$. Since all the states accessible directly by optical excitations can be the intermediate states, the intermediate state a set of basis functions as $\{|\Psi_u\rangle, |\Psi_f\rangle\}$. Then, from (1.18) and (2.50), we have

$$\begin{aligned} N(\varepsilon_B, \eta\omega) = A \cdot \sum_f \Big| \langle \Psi_f | p_e | \Psi_g \rangle + \sum_{uu'} \langle \Psi_f | V_A | \Psi_u \rangle \langle \Psi_u | \frac{1}{\zeta - H - V_A} | \Psi_{u'} \rangle \cdot \\ \langle \Psi_{u'} | p_e | \Psi_g \rangle + \sum_{uf'} \langle \Psi_f | V_A | \Psi_u \rangle \langle \Psi_u | \frac{1}{\zeta - H - V_A} | \Psi_{f'} \rangle \cdot \\ \langle \Psi_{f'} | p_e | \Psi_g \rangle \Big|^2 \times \delta(E_g - E_f + \eta\omega) \delta(E_g - E_f(N-1) + \varepsilon_B) \end{aligned} \tag{2.94}$$

$$\zeta = \eta\omega + E_g + i0^+ \tag{2.95}$$

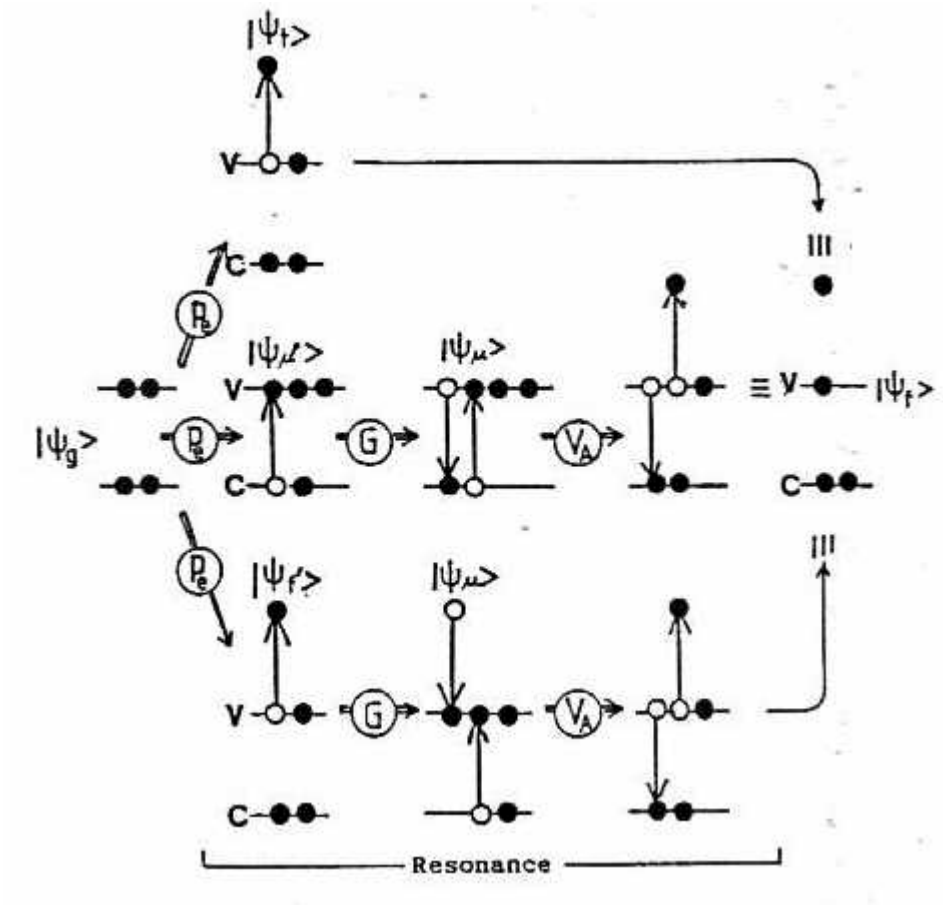

Figure 2.14 Schematic illustration of the resonant photoemission processes, expressed as the propagation of the state occurring in the transitions. V and C stand for the valence level and the core level, respectively.

The terms in the first factor in (2.94) have straight forward meanings. They are illustrated in Fig 2.14. Each state is represented by hypothetical energy levels, where V stand for the valence level, C for the core level, black dots for electrons, white dots for holes, thin arrows for transitions, and thick arrows for propagations. Encircled capital letters represent operators, where G stands for $(\zeta - H - V_A)^{-1}$. Then first line in the figure corresponds to the first term in the first factor in (2.94), the second line to the second term, and the third line to the third term. The second and the third lines represent the resonance. The optical absorption bring about the intermediate state, the propagator G transfer the intermediate state to other intermediate state, and finally the Auger process carries the state to the final goal.

The line shape is approximated by the line shape function known as the Fano (Fano, U. 1961) line shape. It is given as

$$f(\varepsilon) = \frac{(\varepsilon + q)^2}{\varepsilon^2 + 1} \tag{2.96}$$

$$\varepsilon = \frac{\eta\omega - \eta\omega_j}{\Gamma}. \tag{2.97}$$

$$\Gamma = \pi V(\varepsilon) \tag{2.98}$$

where $\eta\omega_j$ is a photon energy equal to the binding energy of core level (near which the resonance is investigated), q is a parameter for the particular core level and $V(\varepsilon)$ represents the interaction potential between the core hole and the outershell electron. For the transition between 3p and 3d, the parameters q and Γ are given as

$$q = \frac{\langle 3d | p_e | 3p \rangle}{\pi \langle 3p, \varepsilon l | e^2/r_{12} | 3d, 3d \rangle \langle \varepsilon l | p_e | 3p \rangle} \tag{2.99}$$

$$\Gamma = \pi \langle \varepsilon l, 3p | e^2/r_{12} | 3d, 3d \rangle \tag{2.100}$$

Resonant photoemission is very useful to draw out the partial density of states curve with a specific symmetry. This is a typical analysis using difference spectrum which is formed by subtracting the off-resonance spectrum from the on-resonance spectrum. The analysis of the resonance process itself is also quite interesting from the view point of physics about the interaction of radiation with condensed matter.

Figure 2.15 shows us the valence-band PE of Ni metal with photon energy around the 3p core level binding energy. It is clear that the 6-ev satellite is enhanced at the photon energy 67eV around 3p threshold. At this photon energy direct photoemission from the valence band (assuming screening by 4s-electron) may be described by (omitting the work function)

$$3d^9 + \eta\omega \rightarrow 3d^8[4s] + e^-[E_{kin} = \eta\omega(E_{3p}) - E_{sat}(valence)]$$

([4s] is a 4s screening electron). This is the 6ev satellite.

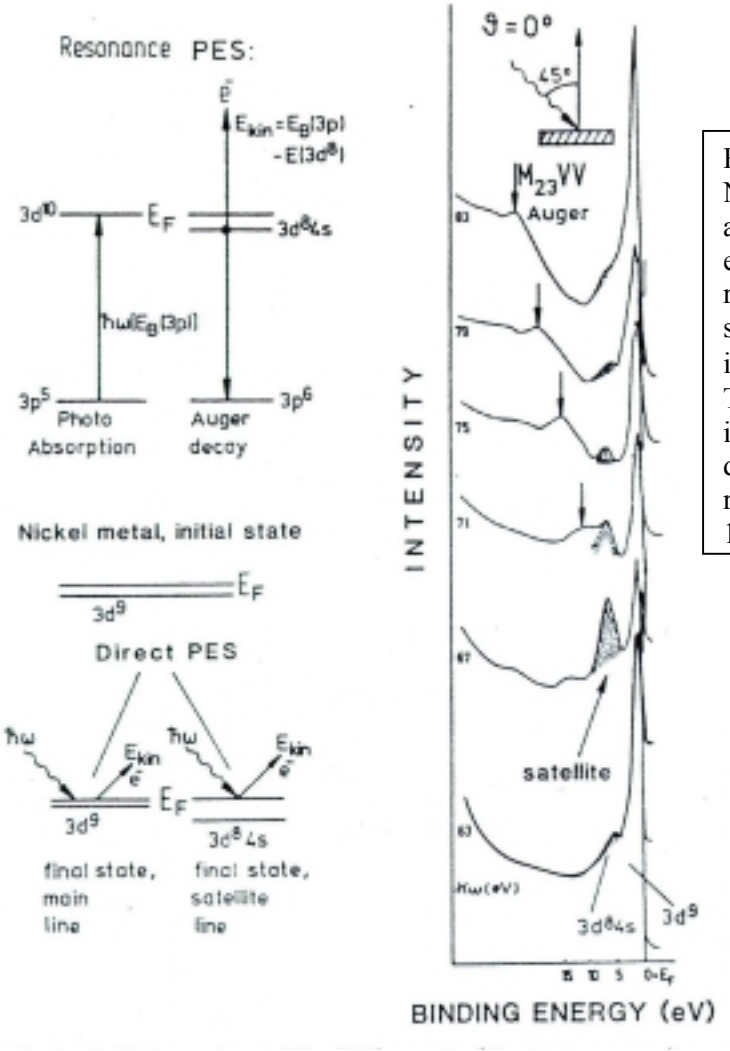

Figure2.15. Valence-band PE of Ni metal with photon energies around the 3p core level binding energy (E_B=67eV). The resonance enhancement of the satellite (hatched area) (E_B=6eV) is clearly seen at $\eta\omega \cong 67eV$. The diagrams on left-hand side indicate the process involved in direct PES (bottom) and resonance PES (top). (Guillot, C. 1977)

In addition, this photon energy can excite an electron from 3p shell into 3d hole just above the Fermi energy in Ni metal and a excited state is formed. The excited state can decay by an Auger process. It leads to the same final state ($3d^8[4s]$) and gives electrons with the same kinetic energy as direct photoemission. We express this process (omitting the work function)

$$3p^6 3d^9 + \eta\omega \rightarrow 3p^5 3d^{10} \xrightarrow{Auger} 3p^6 3d^8[4s] + e^-[E_{kin} = E_{3p} - E_{sat}(valence)]$$

The intensity of the 6ev satellite below the valence band as a function of photon energy is also showed by Figure 2.16.

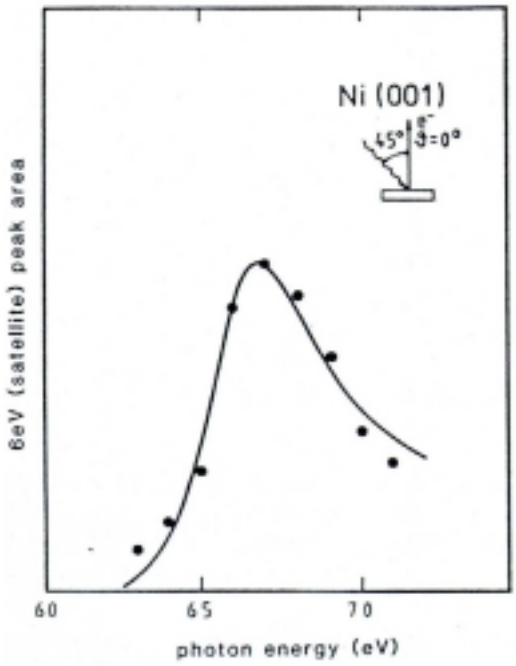

Figure 2.16. Intensity of the satellite 6eV below the valence band as a function of photon energy ($\eta\omega$). (Guillot, C. 1977)

If we arrange an experimental system in which a crystalline sample with a definite crystal plane as the surface and its orientation is fixed in space relative to an energy analyzer and the direction of incident light, we can carry out a typical Angle resolved photoemission (ARPES) and map the dispersions of energy bands. The energy states of metal are characterized by the single-electron energies ε and their wave vectors k, which the $\varepsilon(\mathbf{k})$ relation is the band structure. PES measures transitions between states in occupied and empty bands. These transitions are vertical in a reduced zone scheme (energy and wave vector conservation by neglecting the photon momentum) and called vertical or direct transitions. In this process, a reciprocal vector $\mathbf{G}$ is involved, then, the momentum of potoexcited electron $\mathbf{k}$ should be written as

$$\mathbf{k'} = \mathbf{k} + \mathbf{G} .$$

Consider the third step in three-step model, the transmission of the photoexcited electrons into vacuum must satisfy the condition

$$(\frac{\eta\omega}{2m})\mathbf{k}_{\perp}^{2} > e\varphi \qquad (2.101)$$

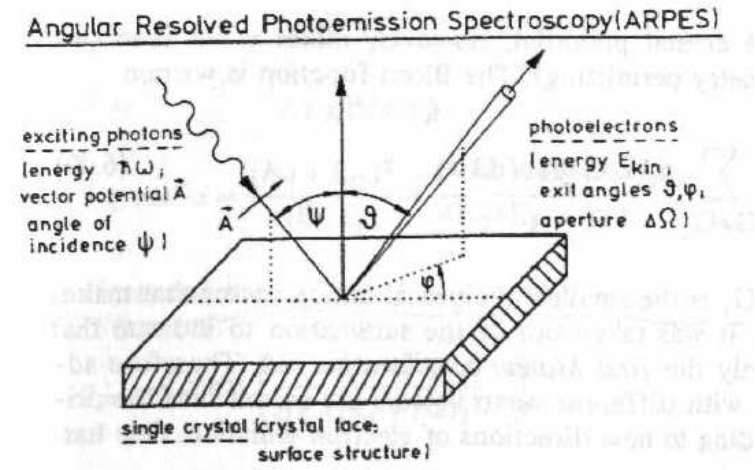

Figure 2.17 Definition of the parameters in an angle-resolved PE (ARPE) experiment; $\eta\omega$: photon energy, A : vector potential of the radiation, Ψ : angle of incidence of photon, θ : polar angle of the detected electrons, φ : azimuthal angle of the detected electrons with respect to the crystal axes, $\Delta\Omega$: detector acceptance angle. (*Hüfner* , S. 1996 pp.362)

The transmission leaves the parallel component of the wave vector conserved

$$\mathbf{p}_{//}/\eta = \mathbf{k'}_{//} = \mathbf{k}_{//} + \mathbf{G}_{//} \qquad (2.102)$$

Here $\mathbf{p}$ is the momentum of the photoelectron in vacuum, $\mathbf{k}_{//}$ is the parallel component of the wave vector $\mathbf{k}$ of the photoexcited electron. So, the kinetic energy outside the crystal is determined by

$$\varepsilon_k = \frac{\eta^2}{2m}[\mathbf{k}_{//}^2 + (\frac{\mathbf{p}_\perp}{\eta})^2] \qquad (2.103)$$

where the $\mathbf{p}_\perp/\eta$ is the perpendicular component of the electron vector in the vacuum. It is clear, that an experiment taken at any $\mathbf{k}_{//}$ does not allow the determination of the full wave vector $\mathbf{k}$ of the crystal state, because $\mathbf{k}_\perp$ remains undetermined. According to this, we have

$$\mathbf{k} = \frac{1}{\eta}\sqrt{2m(\varepsilon_u - e\varphi)}\sin\theta \qquad (2.104)$$

where the θ is the polar angle determined by the direction of the photoelectron as shown in Fig 2.17, the Angle-resolved photoemission experimental scheme. Thus the dispersion of the energy band is obtained, as

$$\varepsilon_{vk} = \varepsilon_v(\mathbf{k}_{//}) . \tag{2.105}$$

Suppose, for example, photoelectrons with high energies just as the XPS case. Then, in the first Brillouin zone, there are many equi-energy surfaces $\varepsilon_{ck'}$ which have the same energy as $\varepsilon_k + \eta\omega$. Thus, there are many cross lines between the equi-energy surfaces $\varepsilon_{ck'}$ and the equi-energy surfaces ε_{vk}. If we draw vectors from the origin to these cross lines, we obtain wave vector **k'** satisfying the energy conservation given by

$$\varepsilon_{ck'} = \varepsilon_{vk} + \eta\omega . \tag{2.106}$$

If we add various G to the vectors obtained above, we have the wave vectors **k'** satisfying both the energy and the momentum conservation given by (2.53) and (2.106). Since we have many equi-energy surfaces and G, we have many different final-state **k'** vectors occurring near the same direction. With a finite angular and energy resolution, different **k'** vectors bing oriented comparatively closely can not be resolved. For small excitation energies, the transition matrix element occurring in (2.54) is small for the transitions in which G is not vanishing. If $G = 0$, the number of **k** satisfying both (2.53) and (2.106) is limited, and ARPES makes sense. The interpretion of the experiment is also illustrated in Fig 2.18.

For metals, the current band structure calculations give reasonable results. But very convenient step consists in approximating the calculation final states by a free-electron parabola. This process can be iterated using the experimental data to adjust the zero of the final state parabola. In a standard method, the only way to change k in order to map the band structure is to change the electron detection angle θ with respect to the surface normal. The analysis of the data is mostly done by so-called

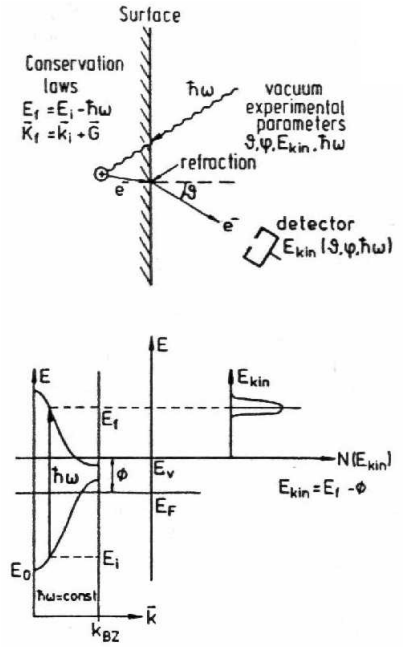

Figure 2.18 PE experiment on a solid as viewed in real space (top) and in momentum space (bottom). (*Hüfner* , S. 1996 pp.264)

"structure plots". In its simplest form this means that one calculates the band structure for the energy and angles used in the experiment and compares an experimental $E(\theta)$ with the theoretical $E(\theta)$. Figure 2.19 shows the results of an experiment with Ne radiation ($\eta\omega = 16.85\text{eV}$) for Ni (110) crystal. The electron detection angle was tilted towards the [111] and [100] direction. The points in Fig 2.19 are directly taken from the EDCs. The theoretical curves were obtained by using a band structure paramatrized in an interpolation scheme for the occupied bands and a free electron final state. The final result of this procedure is presented in Figure 2.20.

We can find from (a) the best fit experimental band structure as obtained from the procedure just outlined and compares it to the available normal emission data obtained using synchrotron radiation. In the right hand panel (b) the experimental band structure is compared to a theoretical one. The deviation between theory and experiment, especially for the d-band width, is quite large. It is believed to come from a considerable final state interaction. But, it is still clear that the density of 3d states is much higher than the density of 4s states. (*Hüfner* , S. 1996 and Huff, W.R.A. 1997)

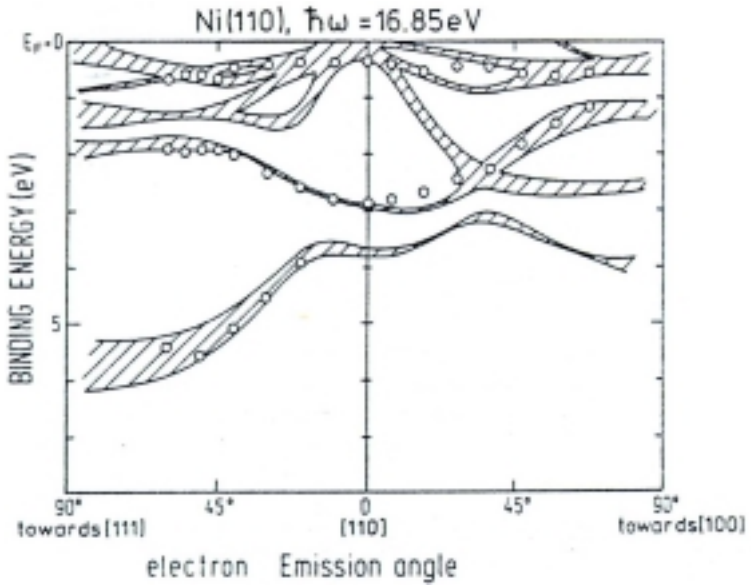

Figure 2.19 "Structure plot" of the valence band of Ni obtained with $\eta\omega = 16.85eV$ from a Ni(110) crystal; the electron detection angle is tilted toward the [111] direction and the [110] direction. The hatched bands are obtained using and interpolation scheme to fit a band structure of Ni to the data points (open dots); the width of the "bands" reflects a 4eV broadening (lifetime) introduced into the final state. (Martensson, H. 1984)

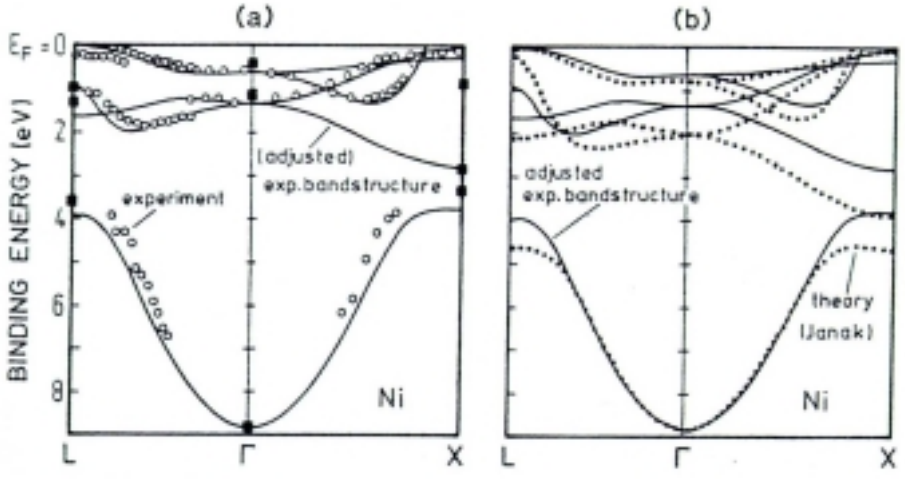

Figure 2.20 "Experimental" band structure of Ni derived with the procedure outlined in Fig2.11 (full curves) (a). Comparison with normal emission PES data (open dots) (b) (dotted curves) calculated band structure. (Martensson, H. 1984)

2.4 Electric Conductivity of Metallic Nickel

All photoemission spectrum showed above tell us the fact that for transition metal elements, they are different from normal metals because of the incompletely filled d level in the crystalline state. Particularly for nickel, the 4s electrons can occupy the empty 3d band with a appropriate probability and the 3d band appears a very large density of states.

According to the facts of nickel, from (2.42), the electric conductivity should be written as:

$$\sigma = \frac{n_e e^2 \tau_e}{m_{se}^*} + \frac{n_h e^2 \tau_h}{m_{dh}^*} \qquad (2.107)$$

where the n_e and n_h are 4s-electron and 3d-hole density. The τ_e and τ_h are relaxation time of 4s-electron and 3d-hole. The m_{se}^* and m_{dh}^* are effective masses of 4s-electron and 3d-hole. Let's consider the scattering probability of 4s-electron and 3d-hole. (Fang, J-X 1983 and Elliot, S.R. 1998) These are:

$$\frac{1}{\tau_e} = \frac{1}{\tau_{ess}} + \frac{1}{\tau_{esd}} \qquad (2.108)$$

and

$$\frac{1}{\tau_h} = \frac{1}{\tau_{hdd}} + \frac{1}{\tau_{hds}} \qquad (2.109)$$

where the subscripts ss, sd, dd and ds denote the scattering between s-s, s-d, d-d and d-s. Because the density of 3d states is much higher than the density of 4s states, we have

$$\tau_{ess} >> \tau_{esd} \qquad (2.110)$$

then

$$\frac{1}{\tau_e} = \frac{1}{\tau_{ess}} + \frac{1}{\tau_{esd}} \approx \frac{1}{\tau_{esd}}. \qquad (2.111)$$

Obviously,

$$\tau_h < \tau_e \qquad (2.112)$$

Also, from the high density of 3d states, we can obtain $m^*_{dh} >> m^*_{se}$ by (2.43). So, the 3d holes of nickel give a very small contribution to the electric conductivity. That is why Ni has high resistivity than normal metals and even the neighbor copper which has completely filled d band.

Chapter III

Photoemission Spectroscopy and Magnetism of Metallic Nickel

Magnetic materials are widely used in our daily life and the most important class of magnetic materials is the ferromagnets. Ferromagnetic materials have two important characteristics: (1) relatively large magnetizations may be induced in them spontaneously or by comparatively low external fields and (2) these materials may retain their magnetizations when the field is removed. However, there are only few ferromagnetic elements in the periodic table, iron, cobalt, nickel and several of lanthanides. In order to satisfy the demeans for different applications, the study of the mechanism of ferromagnets became an important and interesting work. Being one of the simplest ferromagnets, the study of nickel is very representative and significant. Let's review some theories and concepts about magnets first before photoemission experiment in this chapter.

3.1 Magnetism of Metallic Nickel

As we know, the present of a magnetic material will influent the magnetic flux density, thus the relationship among the magnetization , magnetic susceptibility and macroscopic magnetic field intensity is

(3.1a)

or in C.G.S

(3.1b)

Where is the permeability of free space. Substances with a negative magnetic susceptibility are called diamagnetic. Substances with a positive susceptibility are called paramagnetic.

For paramagentic materials, the magnetic moment of an atom or ion in free space is given by

(3.2)

where the total angular momentum is the sum of the orbital and spin angular momenta.

The constant is the ratio of the magnetic moment to the angular momentum, is called the gyromagnetic ratio or magnetogyric ratio. is called the factor or the spectroscopic splitting factor is defined by

(3.3)

For a free atom the factor is given by the Lande equation

. (3.4)

The Bohr magneton is defined as in CGS and in SI. It is closely equal to the spin magnetic moment of a free electron.

In a magnetic field an atom with angular momentum quantum number has equally spaced energy levels. The magnetization for atoms per unit volume given by

(3.5)

where the Brillouin function is defined by

(3.6)

For , we have

(3.7)

We adopt the second order approximation, then

(3.8)

and the susceptibility is

(3.9)

Here is the effective number of Bohr magnetons, defined as

(3.10)

and the Curie constant

(3.11)

The form (3.9) is known as the Curie law.

In contrast to paramagnetic materials, ferromagnetic substances may be maximum magnetical (reach saturation magnetization) in small or negligible fields at normal temperatures. Weiss hypothesized that the reason of spontaneous magnetic moment in ferromagnet is an internal interaction which tends to line up the magnetic moments parallel to each other. This interaction is called exchange field (molecular field). Such a field could be given by the relationship

(3.12)

where is a constant (mean field constant), independent on temperature. If there is a applied field with paramagnetic susceptibility , one has

(3.13)

The paramagnetic susceptibility is given by the Curie law . Compare (3.12) with (3.13), we find

(3.14a)

or in C.G.S

(3.14b)

Detailed calculations predict

(3.15)

at temperature very close to . The reciprocal susceptibility of nickel is plotted in Fig3.1.

From (3.14) and (3.11), we may determine the value of :

. (3.16)

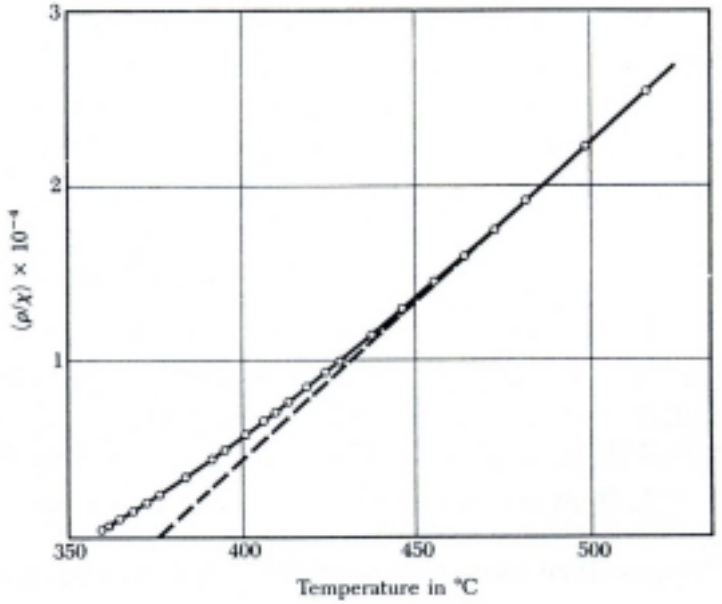

Figure3.1 Reciprocal of the susceptibility per gram of nickel in the neighborhood of the Curie temperature (358 ^{0}c) The density is . The dashed line is a linear extrapolation from high temperature. (Kittle, C. 1986. Pp.425)

Attempts to calculate this exchange field by methods such as the classical Lorentz internal field are too small by a factor of . Thus, the internal field cannot be ascribed to simple magnetic dipole interactions. The modern explanation of exchange field is described under quantum theory. The molecular field postulated by Weiss was “explained” by Heisenberg. Two electrons of spin and are postulated to have a potential energy, in units of , of

(3.17)

Where is the exchange integral that is related to the overlap of the charge distributions and is the angle between their spin vectors.

Ferromagnetism arises from parallel spin ( ) and a positive . Negative values of describe the situation for the antiparallel spin configurations of antiferromagetic and ferrimagnetic materials. Valueof correspond to diamagnetism.

As can be seen from (3.17), the exchange energy and consequently the exchange forces arise from nearest-neighbor interactions. The Pauli principle excludes two electrons of the same spin from being at the same place at the same time. It does not

exclude two electrons of opposite spin. Thus the electrostatic energy of system will depend on the relative orientation of the spins. The difference in energy defines the exchange energy. In the other word, According to the Pauli exclusion principle, only two electrons of opposite spin occupy a give state. Changes in the relative directions of two interacting spins must results in changing their spatial charge distributions. One way to picture this is to consider each state as an "orbit". The average "radius" of the "orbit" of an electron with parallel spin will be different from that of one with an antiparallel spin. A reversal of one of the spin must change the orbit of the other electron and the redistribution of the charges give their energy of interaction. For nearest neighbors with parallel spin, this energy is given as (Daniel D.pollack 1990,1993)

(3.18)

For ferromagnetism , the magnetic moment for one spin, in unit of

. (3.19)

Recalling that the product of molecular field and is energy, it follows that

(3.20)

is the energy at the Curie temperature. By means of (3.18) and (3.20),

(3.21)

For spontaneous magnetization, . In order to relate this to the given nearest neighbors, this must be in terms of the corresponding atomic volume . Thus

. (3.22)

Substitute (3.22) into (3.21)

(3.23)

Which is reduced to

. (3.24)

Then we substitute (3.16) into (3.34) again,

(3.25)

For ferromagentism, the above equation may be reduced, for , to

(3.26)

In case of f.c.c crystal, the is 12 and

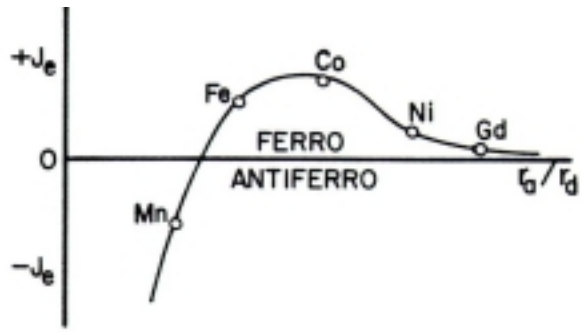

Figure3.2 Schematic diagram of the exchange integral as a function of the ratio of half of the interionic distance to the "radius" of the d band for ferromagnetic elements compared to that of Mn. (Daniel D.Pollack 1990 pp.514)

Another useful result of the exchange theory is postulated by H.Bethe that is a function of , where is the average "radius" of the d shells and is the one-half of the distance between the nuclei of two atoms. So ferromagntism is present when the interionic conditions optimize the overlap of parallel d-level spins. Fig.3.2 shows the relative values of Gd, Ni, Co and Fe, which is known as Bethe-slater

curves. J.C.Slater considered that had to be approximately equal to, but not too much greater than 3.0 for ferromagnetic behavior. His findings show in Table1.

Metal	Cr	Mn	Fe	Co	Ni	Gd
	2.60	2.94	3.26	3.64	3.94	3.1

Table 3.1. (Slater, J.C. 1930)

The alignment of the unbalanced spins gives rise to the magnetic properties of material. The examination of the exchange energy requires a model in which each d band is treaded as two half-band. The electrons in each half-band all have spins of the same direction and all opposite to those in the other half-band. In the nonferromagnetic transition elements, the number of spins in each half-band are equal, in the absence of an external magnetic field, and no net spin imbalance exists. These elements are paramagnetic. Another transition elements like iron, cobalt and nickel contain incomplete 3d levels. The resulting spin imbalance arising form different numbers of electrons in each half-band is responsible for the ferromagnetic behavior of each element.

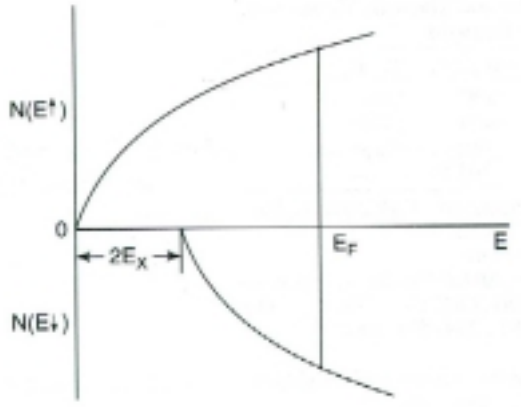

Fihure3.3 Density of states curves for the half-bands of opposite spin. (Daniel D.Pollack 1993 pp.324)

This is shown schematically in Figure.3.3 For the case of nickel, it has the free-atom electronic configuration $3d^8 4s^2$ and the Fermi level lies in the d-band, in contrast to the case of non-magnetic Cu ($3d^{10} 4s^1$) where Fermi level lies midway in the s-band, above the, now-filled, d-band. Of the ten conduction electrons per nickel atom, five completely fill the lower 3d sub-band, but only 4.46 electrons occupy the upper 3d

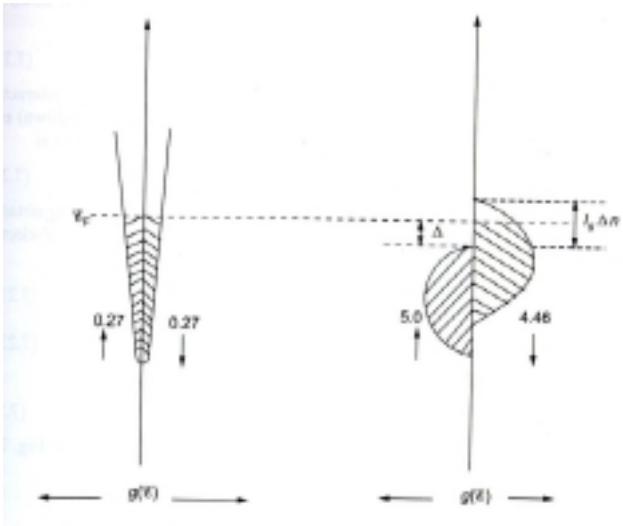

Figure3.4 In Ni, the exchange interaction causes a displacement in energy of the 3d density of states according to the electron-spin direction, but a negligible displacement of the 4s states spin states. The gap, , is the energy separation between the Fermi level and the upper edge of the majority-spin band. Of the 10 electrons per atom, 5 completely fill the lower 3d band and 4.46 occupy the upper 3d band; the remaining 0.54 of an electron per atom is in the 4s band. Thus, there is a net magnetic moment of 0.54 per atom due to the imbalance in the 3d spin populations. (Elliott, S.R 1998 pp.615)

band; the remaining 0.54 of an electron is distributed (approximately equally) between the 4s and 4s bands (for which the exchange splitting is negligible). Thus, there is a net magnetic moment of 0.54 per atom (pointing in the [111] direction) resulting from the difference in the populations of spin-up and spin-down 3d-electrons (or equivalently the presence of the 0.54 of a hole in the 3d band). This value is close to the absolute-zero value of atomic magnetic moment for Ni of 0.6 , the small difference being due to orbital angular momentum contributions. See Figure3.4.

Assume that one half-band contains n more electrons than the others. In terms of the Weiss field

(3.27)

and the internal molecular field is given by

(3.28)

where the is the molecular field. By summing the tendency for parallel spin formation, exchange energy can be expressed:

(3.29)

If is treated as a constant, the transfer of electrons form spin up to spin down effectively lowers the energy of the top of the density of states of the spin up half-band and raises that total difference in the energy between the bands is

(3.30)

The excess number of electrons, n, now equals 2. Because the first half-band lost an electron and the second half-band gained an electron, so

(3.31)

The decrease in is a result of the transfer of an electron from one half-band to another of opposite spin. For this to be the case for spontaneous electron transfer.

(3.32)

In addition, from the equation about nearly free electron

(3.33)

we can easily find the solution

(3.34)

Then the energy difference along the wave vector is

(3.35)

So that the effects of changes in the direction of magnetization are given by

(3.36)

They become functions of the wave vectors. That wave vector providing the optimum lowering of (greatest negative value of) defines the crystallographic direction of easiest magnetization in the crystal, and is the anisotropy energy. This explains why the spontaneous magnetizations of nickel are different for different crystal directions as indicated in Fig3.5.

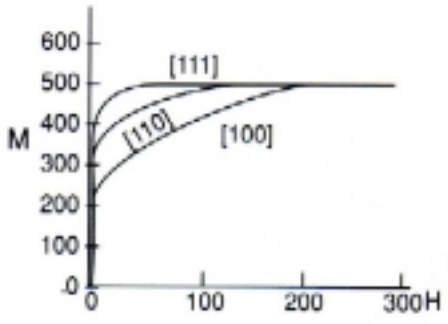

Figure3.5 Magnetization curves of nickel. The easiest directions for spontaneous magnetization are those with the largest values o M for H=0. (Daniel D.Pollock 1993 pp.327)

3.2 Photoemission Spectroscopy of Metallic Nickel

We have mentioned the general theories, which give us the physical explanation for magnetism, especially in ferroemagnetism. From photoemission spectroscopy, a good agreement is presented. Polarized photoelectron spectroscopy is employed. There are two modes in which a PE experiment can produce a spin polarization of the photoemitted electron. One can use unpolarized light to excite polarized electrons in a sample or employ circularly polarized light to excite transition between states that are split by spin-orbit interactions, there by obtaining spin-polarized electrons in the final state. In order to detect electron spins, we use either the Mott scattering technique or the low energy electron diffraction technique. In both methods, a target material is bombarded with electrons to be analyzed and scattered or diffracted electrons are detected. If incident electrons are spin polarized, the intensity of scattered electrons is not uniform along all direction in space. In the case of the Mott scattering, electrons are first accelerated up to about 100keV and then hit the target usually made of Au foil. The number of electrons scattered to the left direction by a fixed angle is different from that scattered to the right direction by the same angle , then the spin polarizability is given as

(3.37)

Here is a quantity called the Sherman function and is known for typical target materials. The spin polarization is defined as

(3.38)

with and being the number of up- and down-polarized electrons. The density of states for electrons with up-spins and that with down-spins

Figure3.6 Photoemission just above the threshold ( ) for Ni. Under these conditions only minority spin (spin down) photoelectrons can be observed. (Eib, W. 1976)

are obtained from the spin polarizability and the density of states without spine analysis, as

(3.39)

(3.40)

thus, we are able to obtain spin resolved DOS curves or EDC's from the spin polarizability and spin unresolved DOS curves or EDC's.

Figure.3.6 shows the schematic density of states of ferromagnetic Ni. This is an oversimplification (rigid band splitting) and overlook the exchange the wave vector dependence of the exchange splitting energy. A critical test was made by measuring the spin polarization of electrons photoemitted for Ni near the photothreshold. The results are shown in Fig.3.7. We can find that the spin polarization of the 3d photoemission was measured as a function of the incident photon energy. When the photon energy is sufficiently close to the work function (so that the photoelectron is excited from the state sufficiently close to . It also means minorty-spin electrons are excited with a high probability) the "observed" is negative, at a value of photon energy which is much smaller than the estimated from the band theory. It was show by Moore and Pendry that in order to reproduce the experimental versus photon energy relation the exchange splitting obtained form self-consistent energy band

Figure3.7 Measurement of the spin polarized PE from Ni(100) at T=273K. Near threshold a negative spin polarization is observed as expected (Fig.3.6). On increasing the photon energy one also probes the states further below E_F and thus the resulting spin polarization becomes positive. (Eib, W. 1976)

calculations, because of the electron correlation effect is not taken into account sufficiently in the energy band theory. (, S 1996)

Himpsel (1979) observed the angle-resolved photoelectron spectra from the valence band of Ni, and succeeded to obtain experimentally the energy dispersion of 3d and 4s electrons along several high-symmetry axes in the wave vector space. They estimated the exchange splitting from their experimental energy separation of a pair of exchange-split branches near the L_3 point and obtained eV, in good agreement with the given by Moore and Fendry. (Akio Kotani 1987 and Greber, T. 1997)

Recall the 6-ev satellite, which we have mentioned in the pervious chapter, it shows a resonance enhancement at the 3p photothreshold because direct photoemission and the Super-Koster-Kroning Auger decay in the valence band. For the case of Ni, the Auger electrons should be polarized, as can be understood with reference to Fig.3.8 .

At threshold photoabsorption ( ) only spin-down (minority) electrons are photoexcited, since only the spin down band has empty states at the Fermi energy. These results in an intermediate “spin-up” polarized state with a “spin-down” hole in the 3p shell. The deexcitation process leads to the final $3d^8$ state in the valence band, takes place via the emission of two electrons out of the valence band.

Figure3.8 Spin polarization for the 6eV satellite in Ni metal measured at threshold for the photoexcitation of Ni 3p electrons ( ). At threshold there are only empty minority states in Ni metal, and thus only minority holes are produced in 3p shell:

which leads to the decay

.

One should thus measure a positive (spin-up) spin polarization.
(Feldkamp, L.A 1979)

Since the Auger electrons lead to a singlet (S=0) final state and only spin-down electrons can go into the $3d^5$ state, spin-up electrons must be ejected. As the data in Fig3.9 demonstrate, a positive spin polarization ( ) is indeed observed experimentally. This provides further evidence to support the picture of the nature of the 6ev satellite in Ni metal.

Although less directly, the same kind of information has been obtained from a normal (non-spin-ploarized) PE experiment. Two spectial spectra are given in Fig.3.10. In this case one must assume from the out set that the small splitting observed is due to the exchange splitting of the band, since the experiment itself cannot discriminate between spin-up and spin-down electrons. These spectra are also satisfied the relation shown in Fig 3.5.

So, it is clear that the exchange splitting is observed very well in photoemission spectroscopy. It supports the theoretical explanation for ferromagentism.

Figure3.9 Measurement of the spin polarization of the 6eV satellite at threshold ( ). (a) EDC at resonance; (b) polarization (positive) as measured; (c) polarization corrected for background. (Raue, R 1983)

Figure3.10 Analysis of high-resolution spectra of Ni. The larger binding energy component shows a greater width due to the larger Auger decay rate. (Heimann, P. 1981)

Chapter IV

Conclusion

Photoemission Spectroscopy has been used for the studies of the electronic structure of materials. We found that the reported PES of metallic nickel convincingly supports the theoretical explanation about its poor electrical conductivity and ferromagnetism. These physical properties are determined by the electronic structure essentially, which is difficult to investigate through another experiments.

From the core-level and resonance photoemission spectroscopy, the spectrum, 6-ev satellite, demonstrates the two-hole can be scattered into 3d band by electron-electron interaction. Therefore, both the 4s electrons and 3d holes give the contribution for the electrical conductivity. Further information is obtained by angular-resolved spectroscopy. Metallic nickel has a narrow 3d energy band with a very high level lies within them. Theoretical analysis regards that the narrow 3d band leads a large effective mass of 3d-hole and a short relaxation time. These satisfy the fact that nickel has high electrical resistivity.

Modern photoemission techniques open a new way to investigate a material involving quantum numbers. The imbalance of electron spin in the 3d band of nickel is shown by so-called spin-ploarized photoemission spectroscopy. The exchange energy which is various with the crystallchraphic direction is also visible, whereas we found that the exchange splitting energy is only a half of the theoretical calculation because of the defect in the energy band theories. But is could not affect our understanding for the ferromagnetism of nickel, which is that the spontaneous magnetic moment appears in the absence of an applied magnetic field due to the spin-up and spin-down bands are shifted with respect to one another by the exchange splitting below the Curie temperature.

In the present thesis, we mainly overviewed the application of PES in metallic nickel due to limited space. Despite the limitation, the advantage of PES is still shown greatly. It is very helpful for us to understand and investigate other materials, especially the alloys and compounds of transition metals.

References

Akio Kotani (1987). **Inner Shell Photoelectron Process in Solids**. Handbook on Synchrotron Radiation, Vol.2, Elsevier Science Publishers B.V.

Bleaney, B.I. and Bleaney, B. (1992). **Electricity and Magnetism** (3rd ed.), Vol.2, Oxford Universtity Press.

Campagna, M. (1985). **J. Vac. Sci. Technol.** A3: 1491. Quoted in *Hüfner* , S. (1996). **Photoelectron spectroscopy** (2nd ed.). New York: Springer-Verlag.

Daniel, D. Pollack (1990). **Physics of engineering materials.** Prentice-Hall International.

Daniel, D. Pollack (1993). **Physical properties of materials for engineers** (2nd ed.). CRC Press.

Eib, W. and Alvarado, S. F. (1976). **Phys. Rev. Lett.** 37: 444. Quoted in *Hüfner* , S. (1996). **Photoelectron spectroscopy** (2nd ed.). New York: Springer-Verlag.

Elliott, S. R. (1998). **The physics and chemistry of solids.** John Wiley & Sons.

Fang, J-X. and Lu, D. (1983). **Solid state physics.** Shanghai Academic Press (in Chinese).

Fano, U. (1961). Phys. Rev. 124: 1866. Quoted in *Hüfner* , S. (1996). **Photoelectron spectroscopy** (2nd ed.). New York: Springer-Verlag.

Feldkamp, L. A. and Davis, L. C. (1979). **Phys. Rev. Lett.** 43: 151. Quoted in *Hüfner* , S. (1996). **Photoelectron spectroscopy** (2nd ed.). New York: Springer-Verlag.

Greber, T., Kreutz, T. J., and Ostemalder, J. (1997). Photomission above the Fermi level: The top of the minority d band in nickel. **Phys. Rev. Lett.** 78: 4465-4468.

Guillot, C., Ballu, Y., Paigne, J. and Jain K. P. (1977). **Phys. Rev. Lett.** 39: 1632. Quoted in *Hüfner* , S. (1996). **Photoelectron spectroscopy** (2nd ed.). New York: Springer-Verlag.

Heimann, P., Himpsel, F. J. and Eastman, D. E. (1981). **Solid State Commun.** 39: 219. Quoted in *Hüfner* , S. (1996). **Photoelectron spectroscopy** (2nd ed.). New York: Springer-Verlag.

Himpsd, F. J. (1995). Photoemission and photoelectron spectra. **Encyclopedia of applied physics**. 13: 478.

Huff, W. R. A., Chen, Y., Kellar, S. A. and Moler, E. J. (1997). Angle-resolved photoemission extended fine structure of the Ni 3p, Cu 35, and Cu 3p core levels of the respective clean (111) surfaces, **Phy. Rev. B**56: 1540-1550.

Hüfner , S. (1996). **Photoelectron spectroscopy** (2nd ed.). New York: Springer-Verlag.

Hüfner , S. and Wertheim, G. K. (1978). **Phys. Lett**. 51**A**: 299. Quoted in *Hüfner* , S. (1996). **Photoelectron spectroscopy** (2nd ed.). New York: Springer-Verlag.

Johansson, B. and Martensson, N. (1980). **Phys. Rev. B**21: 4427. Quoted in *Hüfner* , S. (1996). **Photoelectron spectroscopy** (2nd ed.). New York: Springer-Verlag.

Kittle, C. (1986a). **Introduction to solid state physics** (6th ed.). John Wiley & Sons.

Lbach, H. (1977). **Electron Spectroscopy for Surface Analysis.** Quoted in *Hüfner* , S. (1996). **Photoelectron spectroscopy** (2nd ed.). New York: Springer-Verlag.

Martensson, H. and Nisson, P. O. (1984). **Phys. Rev.** B30: 3047. Quoted in *Hüfner* , S. (1996). **Photoelectron spectroscopy** (2nd ed.). New York: Springer-Verlag.

Myers, H. P. (1977). **Introductory solid state physics** (2nd ed.). Taylor & Francis.

Raue, R., Hopster, H., and Clanberg, R. (1983). **Phys. Rev. Lett.** 50: 1623. In Quoted in *Hüfner* , S. (1996). **Photoelectron spectroscopy** (2nd ed.). New York: Springer-Verlag.

Sakurai, J. J. (1994). **Modern quantum mechanics.** Addison-Wesley.

Slater, J. C. (1930). **Phys. Rev.** 36: 57. Quoted in Daniel, D. Pollack (1990). **Physics of engineering materials.** Prentice-Hall International.

Zornberg, E. J. (1970). **Phys. Rev. B**1: 244. Quoted in *Hüfner* , S. (1996). **Photoelectron spectroscopy** (2nd ed.). New York: Springer-Verlag.

Appendix A

Brillouin Zone of the Three Low-Index Face of Face-Centered Cubic (fcc) Crystal Face

Brillouin gave the statement of the diffraction condition that is most widely used in solid state physics, which means in the description of electron energy band theory and of the elementary excitations of other kinds.

Reciprocal Lattice to fcc Lattice

The primitive translation vector of the fcc lattice of Fig. A1 are

$$\mathbf{a}_1 = \frac{1}{2}a(\hat{\mathbf{y}} + \hat{\mathbf{z}}); \quad \mathbf{a}_2 = \frac{1}{2}a(\hat{\mathbf{x}} + \hat{\mathbf{z}}); \quad \mathbf{a}_3 = \frac{1}{2}a(\hat{\mathbf{x}} + \hat{\mathbf{y}}).$$

The volume of the primitive cell is

$$V = \left|\mathbf{a}_1 \cdot \mathbf{a}_2 \times \mathbf{a}_3\right| = \frac{1}{4}a^3.$$

The primitive translation vectors of the lattice reciprocal to the fcc lattice are

$$\mathbf{b}_1 = (2\pi/a)(-\hat{\mathbf{x}} + \hat{\mathbf{y}} + \hat{\mathbf{z}}); \quad \mathbf{b}_2 = (2\pi/a)(\hat{\mathbf{x}} - \hat{\mathbf{y}} + \hat{\mathbf{z}});$$

$$\mathbf{b}_3 = (2\pi/a)(\hat{\mathbf{x}} + \hat{\mathbf{y}} - \hat{\mathbf{z}}).$$

These are primitive translation vectors of a bcc lattice, so that the bcc lattice is reciprocal to the fcc lattice. The volume of the primitive cell of the reciprocal lattice is $4(2\pi/a)^3$.

The shortest **G** 's are the eight vectors

$$(2\pi/a)(\pm\hat{\mathbf{x}} \pm \hat{\mathbf{y}} \pm \hat{\mathbf{z}})$$

The boundaries of the central cell in the reciprocal lattice are determined for the most part by the eight planes normal to these vectors at their midpoints. But the corners of the octahedron thus formed are cut by the planes that are the perpendicular bisectors of six other reciprocal lattice vectors:

$$\left(2\pi/a\right)(\pm 2\hat{\mathbf{x}}); \quad \left(2\pi/a\right)(\pm 2\hat{\mathbf{y}}); \quad \left(2\pi/a\right)(\pm 2\hat{\mathbf{z}}).$$

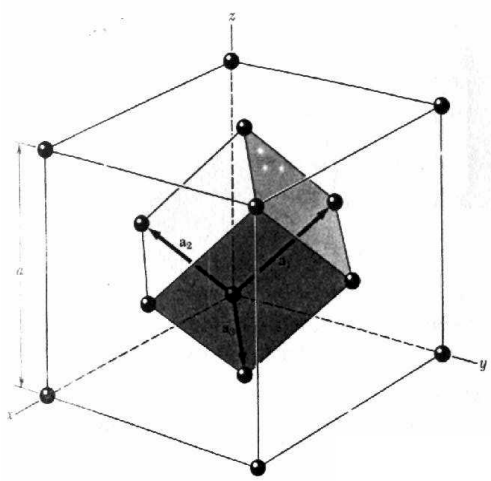

Figure A1. Primitive basis vectors of the face-centered cubic lattice.

Note that $\left(2\pi/a\right)(2\hat{\mathbf{x}})$ is a reciprocal lattice vector because it is equal to $\mathbf{b}_2 + \mathbf{b}_3$. The first Brillouin zone is the smallest bounded volume about the origin, the truncated octahedron shown in Fig. A2. The six planes bound a cube of edge $\left(4\pi/a\right)^3$. (See Kittel, C. 1986, Chapter 2)

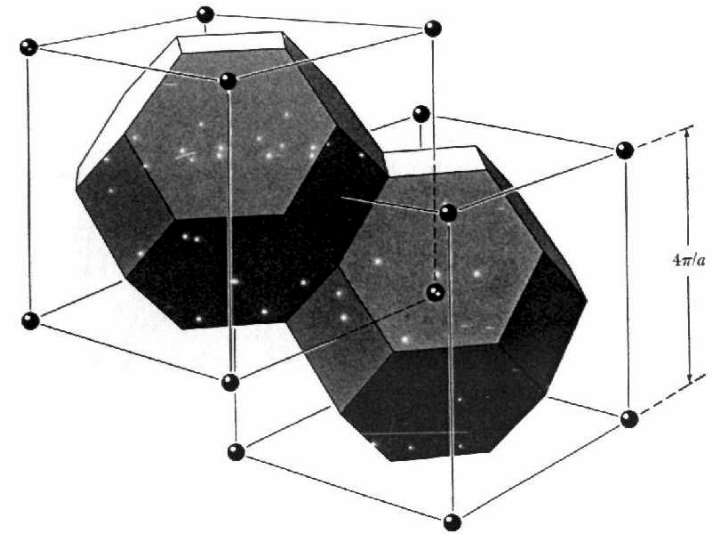

Figure A2. Brillouin zones of the face-centered cubic lattice. The cells are in reciprocal space, and the reciprocal lattice is body centered.

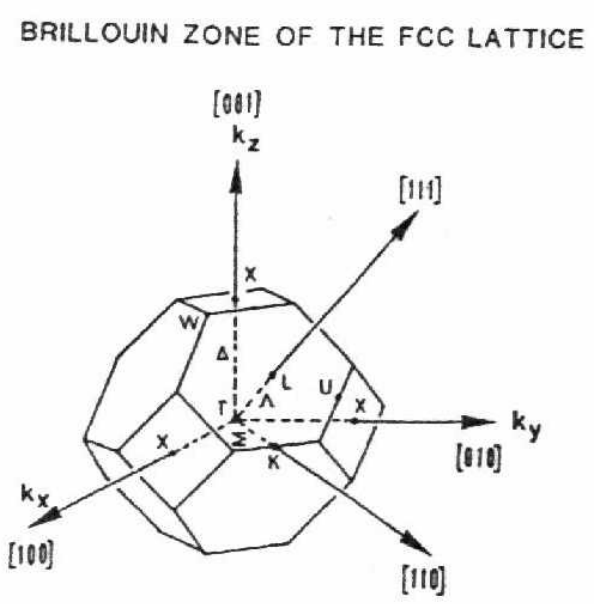

Figure A3. Some symmetry points in Brillouin zone:

	Γ	X	K	L
Wave vector **k**	$\frac{2\pi}{a}(0, 0, 0)$	$\frac{2\pi}{a}(1, 0, 0)$	$\frac{2\pi}{a}(\frac{3}{4}, \frac{3}{4}, 0)$	$\frac{2\pi}{a}(\frac{1}{2}, \frac{1}{2}, \frac{1}{2})$

Some points on the symmetry axises:

	Δ	Σ	Λ
Wave vector **k**	$\frac{2\pi}{a}(\delta, 0, 0)$	$\frac{2\pi}{a}(\sigma, \sigma, 0)$	$\frac{2\pi}{a}(\lambda, \lambda, 0)$
	$0 < \delta < 1$	$0 < \sigma < \frac{3}{4}$	$0 < \lambda < \frac{1}{2}$

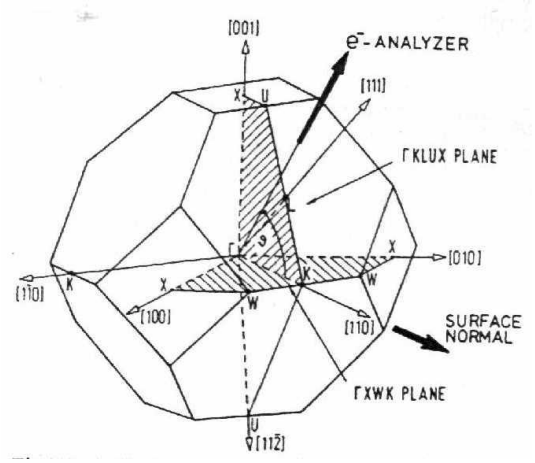

Biography

Mr. Jiang Yang was born on 15th April 1975 in Gui Yang, Gui Zhou, China. In 1993, he went to study in Department of Optics, Institute of Science, at Shandong University, China and graduated in 1997. In 1998, he decided to study for a Master's degree of physics and enrolled in School of Physics, Institute of Science, Suranaree University of Technology.